

Dietary fructose enhances tumour growth indirectly via interorgan lipid transfer

<https://doi.org/10.1038/s41586-024-08258-3>

Received: 18 June 2020

Accepted: 21 October 2024

Published online: 4 December 2024

 Check for updates

Ronald Fowle-Grider^{1,2,3}, Joe L. Rowles III^{1,3}, Isabel Shen^{1,3}, Yahui Wang^{1,3}, Michaela Schwaiger-Haber^{1,3}, Alden J. Dunham^{1,3}, Kay Jayachandran⁴, Matthew Inkman⁴, Michael Zahner^{4,5}, Fuad J. Naser^{1,3}, Madelyn M. Jackstadt^{1,3}, Jonathan L. Spalding^{1,3,6}, Sarah Chiang^{1,3}, Kyle S. McCommis⁷, Roland E. Dolle², Eva T. Kramer^{5,6}, Sarah M. Zimmerman⁵, George P. Souroullas^{5,8}, Brian N. Finck⁹, Leah P. Shriver^{1,3}, Charles K. Kaufman^{5,6}, Julie K. Schwarz^{4,8,10}, Jin Zhang^{4,8,11} & Gary J. Patti^{1,3,8,12} 

Fructose consumption has increased considerably over the past five decades, largely due to the widespread use of high-fructose corn syrup as a sweetener¹. It has been proposed that fructose promotes the growth of some tumours directly by serving as a fuel^{2,3}. Here we show that fructose supplementation enhances tumour growth in animal models of melanoma, breast cancer and cervical cancer without causing weight gain or insulin resistance. The cancer cells themselves were unable to use fructose readily as a nutrient because they did not express ketohexokinase-C (KHK-C). Primary hepatocytes did express KHK-C, resulting in fructolysis and the excretion of a variety of lipid species, including lysophosphatidylcholines (LPCs). In co-culture experiments, hepatocyte-derived LPCs were consumed by cancer cells and used to generate phosphatidylcholines, the major phospholipid of cell membranes. *In vivo*, supplementation with high-fructose corn syrup increased several LPC species by more than sevenfold in the serum. Administration of LPCs to mice was sufficient to increase tumour growth. Pharmacological inhibition of KHK had no direct effect on cancer cells, but it decreased circulating LPC levels and prevented fructose-mediated tumour growth *in vivo*. These findings reveal that fructose supplementation increases circulating nutrients such as LPCs, which can enhance tumour growth through a cell non-autonomous mechanism.

Increasing evidence suggests that dietary fructose promotes the growth of multiple tumour types^{4–8}. To date, the mechanisms by which fructose has been purported to enhance tumour growth have been cell autonomous. Consistent with this reasoning, some malignant human tissues overexpress the fructose transporters GLUT2 and GLUT5⁹. Moreover, under certain conditions, several studies have demonstrated that a number of cancer cells in culture can use fructose for both energy and biomass production^{2,10}. For cancer cells to use fructose directly as a major fuel source, however, fructose must be accessible to the tumour tissue. Most of the fructose from the diet is metabolized by the small intestine and liver^{11–14}. Even with high-fructose diets, only a relatively small amount of fructose enters systemic circulation^{12–14}. This raises the question of whether the growth of tumours residing in tissues in which fructose availability is limited might still be enhanced by directly using dietary fructose. Here we considered a cell non-autonomous mechanism whereby dietary fructose increases tumour growth indirectly by metabolite transfer.

Dietary fructose promotes tumour growth

To first investigate the effects of fructose on the growth of tumours outside of the small intestine and liver, we evaluated a well-established zebrafish model of melanoma¹⁵. Specifically, we used *p53*-deficient fish with a human *BRAF^{V600E}* oncogene under the control of the melanocyte-specific *mitfa* promoter (hereafter, *BRAF/p53* fish). To determine whether fructose increases melanoma growth, we used an assay to evaluate tumour size over time (Extended Data Fig. 1a and Supplementary Fig. 2). After 2 weeks, there was growth of tumours in fructose water, but there was no detectable growth of tumours in control water (Fig. 1a).

Next, we sought to extend our analysis to a model of melanoma in mice. We subcutaneously implanted 300,000 mouse *Braf^{V600E}*-mutant, *Pten*-deficient melanoma cells into female C57BL/6 mice and monitored tumour growth as a function of time. Rather than exposing animals to a sustained level of fructose as we did for fish above, we gave animals

¹Department of Chemistry, Washington University, St Louis, MO, USA. ²Department of Biochemistry and Molecular Biophysics, Washington University School of Medicine, St Louis, MO, USA.

³Center for Mass Spectrometry and Metabolic Tracing, Washington University, St Louis, MO, USA. ⁴Department of Radiation Oncology, Washington University School of Medicine, St Louis, MO, USA. ⁵Division of Medical Oncology, Washington University School of Medicine, St Louis, MO, USA. ⁶Department of Developmental Biology, Washington University School of Medicine, St Louis, MO, USA. ⁷Department of Biochemistry & Molecular Biology, Saint Louis University School of Medicine, St Louis, MO, USA. ⁸Siteman Cancer Center, Washington University School of Medicine, St Louis, MO, USA. ⁹Division of Geriatrics and Nutritional Sciences, Washington University School of Medicine, St Louis, MO, USA. ¹⁰Department of Cell Biology and Physiology, Washington University School of Medicine, St Louis, MO, USA. ¹¹Institute for Informatics, Data Science & Biostatistics (I2DB), Washington University School of Medicine, St Louis, MO, USA. ¹²Center for Human Nutrition, Department of Medicine, Washington University School of Medicine, St Louis, MO, USA.  e-mail: gjpattij@wustl.edu

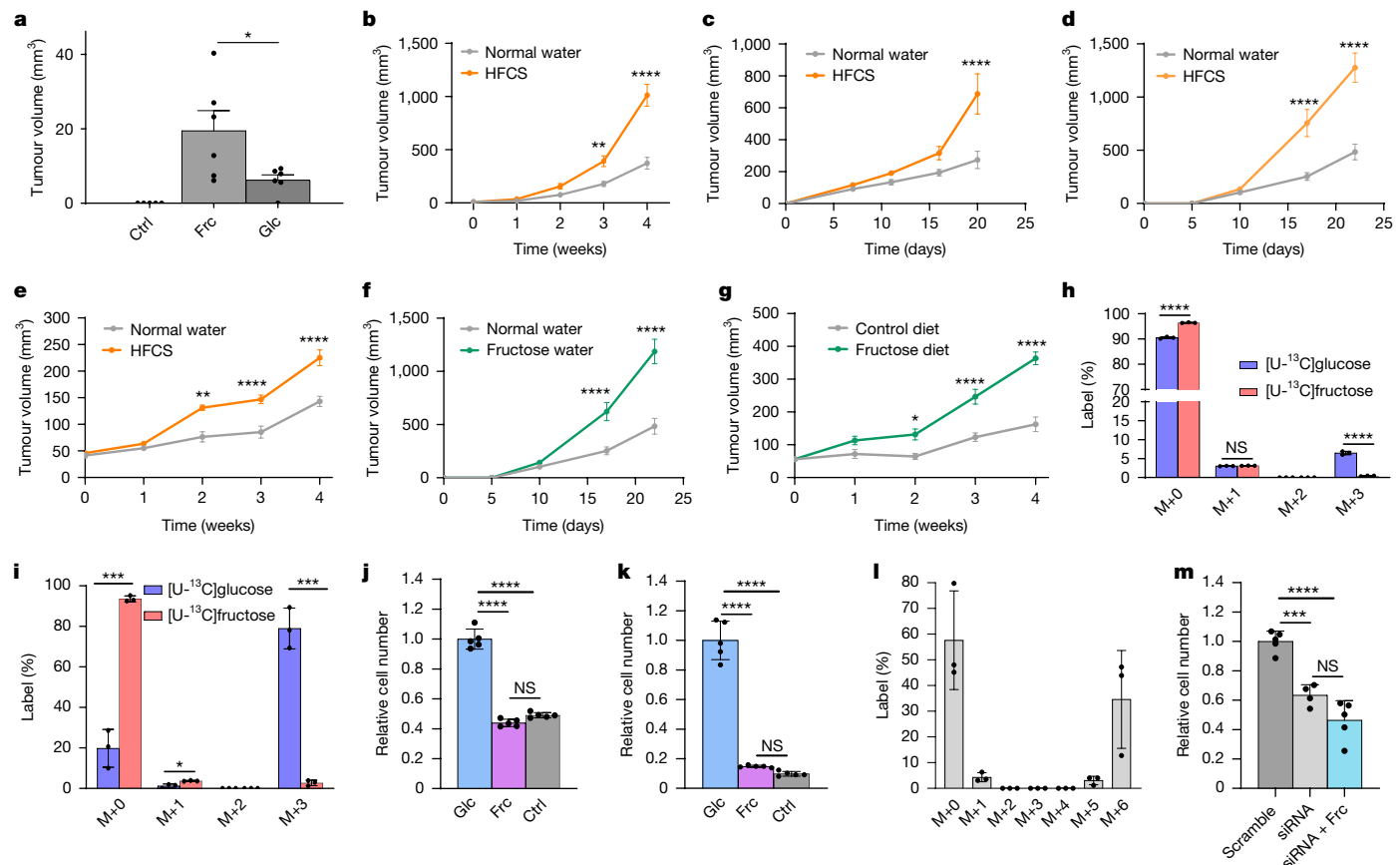


Fig. 1 | Dietary fructose supports tumour growth in vivo but fructose is not efficiently metabolized by cancer cells in vitro. **a**, Tumour regrowth 2 weeks after tumour amputation from *BRAF/p53* zebrafish in control water (Ctrl, $n=5$), water containing fructose (Frc, $n=6$) or water containing glucose (Glc, $n=6$). No regrowth was detected in the control water condition. Data are representative of two experiments. **b–e**, Tumour outgrowth after *Braf^{V600E}*Pten^{-/-} melanoma ($n=7$) (**b**), E0771 cells (normal water, $n=10$ and HFCS, $n=9$) (**c**), E6/E7-expressing TC-1 cells (normal water, $n=16$ and HFCS, $n=13$) (**d**) and CaSki cells (normal water, $n=5$ and HFCS, $n=5$) (**e**) were implanted subcutaneously (**b,d,e**) or into the mammary fat pad (**c**) of mice supplemented with normal water or 20% HFCS water. **f,g**, Tumour outgrowth of subcutaneous E6/E7-expressing TC-1 tumours in mice supplemented with normal water ($n=16$) or 10% fructose water ($n=13$) (**f**) and of subcutaneous CaSki tumours in mice on a control diet ($n=5$) or a high-fructose diet ($n=7$) (**g**). **h,i**, The isotopologue distribution for lactate from *BRAF/p53* zebrafish melanoma cells cultured ex vivo ($n=3$) (**h**) or CaSki cells ($n=3$) (**i**) after 4 h of labelling with

5 mM [$U-^{13}C$]glucose or 5 mM [$U-^{13}C$]fructose. **j,k**, Zcrest C *BRAF/p53* zebrafish melanoma cells ($n=5$ per condition) (**j**) and CaSki cells ($n=5$ per condition) (**k**) were cultured in medium with 10 mM glucose (Glc), 10 mM fructose (Frc) or no sugar (Ctrl). **l**, The isotopologue distribution for endogenous fructose from CaSki cells cultured with [$U-^{13}C$]glucose ($n=3$). **m**, The relative cell number after administering sorbitol dehydrogenase small interfering RNA (siRNA, $n=4$), scrambled control (scramble, $n=5$), or sorbitol dehydrogenase siRNA and 10 mM fructose (siRNA + Frc, $n=5$) to CaSki cells. Except where indicated, experiments in this figure were performed once. P values were determined using unpaired t -tests comparing the fructose and glucose conditions (**a**), two-way analysis of variance (ANOVA) with Šidák's multiple-comparisons test (**b–g**), multiple unpaired t -tests (**h and i**) or ordinary one-way ANOVA with Tukey's multiple-comparisons test (**j, k and m**). * $P<0.05$, ** $P<0.01$, *** $P<0.001$, **** $P<0.0001$; NS, not significant. Data are mean \pm s.e.m (**b–g**) and mean \pm s.d. (**a** and **h–m**).

access to high-fructose corn syrup (HFCS) solution, which is the form of fructose that is most commonly consumed in a Western diet¹⁶. As a control, mice were given standard water and fed a diet resembling normal chow but without any fructose or free sugars (Supplementary Table 1). In the treated condition, water was replaced with a 20% HFCS solution. Consistent with our findings in zebrafish, tumours grew faster in mice with access to HFCS solution (Fig. 1b).

To determine whether this effect is specific to melanoma, we assessed other tumours that reside outside the small intestine and liver. First, we implanted E0771 breast cancer cells into the mammary fat pad of female C57BL/6 mice. Second, we implanted TC-1 cervical cancer cells (expressing HPV-E6 and HPV-E7 proteins) subcutaneously or orthotopically into the cervix of C57BL/6 mice. In all cases, diets supplemented with HFCS resulted in faster tumour growth compared with control diets (Fig. 1c,d and Extended Data Fig. 1b). Relative to the control diets, HFCS supplementation also resulted in increased tumour growth in athymic nude mice bearing subcutaneous CaSki tumours (Fig. 1e).

To confirm that fructose alone is sufficient to promote tumour growth in mice, experiments were repeated with TC-1 and CaSki cells but the mice were either given control diets supplemented with 10% fructose water (Fig. 1f and Extended Data Fig. 1b) or mice were given chow containing fructose (Fig. 1g and Supplementary Table 1). Tumours in mice supplemented with fructose consistently grew faster than tumours in control animals. Taken together, these data demonstrate that dietary fructose increases tumour growth in multiple different tumour models.

Considering the potential for high-fructose consumption to contribute to obesity and insulin resistance^{17,18}, we considered whether changes in tumour growth were secondary to changes in metabolic health (Supplementary Note 1 and Extended Data Fig. 1c–m). We found that fructose promoted tumour growth without changing body weight (Extended Data Fig. 1c,d). Mice on high-fructose diets also had no differences in fasting glucose or fasting insulin levels (Extended Data Fig. 1e–h). These data suggest that, even after 6 weeks, increased fructose consumption did not induce insulin resistance.

Fructose does not directly fuel proliferation

Given the enhanced rate of tumour growth with dietary fructose in multiple tumour types and models, we wanted to test whether fructose might be directly consumed by cancer cells as a fuel to support proliferation. To assess this possibility, we cultured various cancer cells from different tissues of origin in [$U\text{-}^{13}\text{C}$]fructose and monitored its fate by performing metabolomics analysis with liquid chromatography–mass spectrometry (LC–MS) metabolomics. Before performing cell-culture experiments, we aimed to determine physiologically relevant fructose concentrations and culture times (Supplementary Note 2 and Extended Data Fig. 2a). On the basis of these results, we concluded that culturing cells in 5 mM fructose for 4 h would exceed maximum fructose exposure *in vivo*.

We first labelled the following zebrafish, mouse and human cancer cell lines derived from a variety of cancer types (Supplementary Fig. 3) with 5 mM [$U\text{-}^{13}\text{C}$]fructose or 5 mM [$U\text{-}^{13}\text{C}$]glucose in culture for 4 h: *BRAF^{V600E}*-mutant zebrafish melanoma cells; *Braf^{V600E}*-mutant, *Pten*-deficient mouse melanoma cells; E0771 murine breast cancer cells; TC-1 murine cells of lung epithelial origin transfected to stably express the E6 and E7 oncogenes of HPV-16; CaSki human cervical cancer cells; A-498 human renal cancer cells; MIA PaCa-2 human pancreatic cancer cells; 3T3 murine fibroblasts; and MCF7 breast cancer cells. Moreover, we amputated a tumour from *BRAF/p53* zebrafish, formed a single-cell suspension and plated the cells *ex vivo* for cell-culture analysis. We next labelled zebrafish melanoma cells *ex vivo* with [$U\text{-}^{13}\text{C}$]glucose or [$U\text{-}^{13}\text{C}$]fructose. As expected, we saw extensive metabolism of [$U\text{-}^{13}\text{C}$]glucose in all of the experiments as represented by ^{13}C enrichment in lactate (Fig. 1h,i and Extended Data Fig. 2b–k). To the contrary, we observed minimal metabolism of the fructose label in all of the cell lines analysed (Fig. 1h,i and Extended Data Fig. 2b–k). We next assessed the proliferation of cells cultured in 10 mM fructose as the only sugar source in the medium. We used an even higher concentration of fructose than in our previous ^{13}C -labelling experiments to ensure that cells did not deplete the sugar over the time course of the experiment (4 days). Consistent with our ^{13}C -labelling data above, cells incubated in DMEM with 10 mM fructose as the only sugar source proliferated much slower compared with cells cultured in DMEM with 10 mM glucose as the only sugar source (Fig. 1j,k and Extended Data Fig. 3a–j), even though the fructose concentration was supraphysiological. Notably, some cells cultured in fructose did not proliferate much faster than cells in control medium with no sugar added at all (Fig. 1j,k and Extended Data Fig. 3a–j). Plotting CaSki cell number as a function of time revealed that cells in fructose medium proliferate more slowly than in glucose medium, as opposed to fructose acting as a cytotoxic agent (Extended Data Fig. 3k). We confirmed that the limited ability of these cells to metabolize fructose was not due to an inability to uptake it, as all cell lines readily took up the fluorescent analogue of fructose 1-NBDF (Extended Data Fig. 3l–q).

In the majority of physiological contexts, tissues are not exposed to fructose as the only sugar source. Glucose concentrations are typically at least an order of magnitude higher in the serum than postprandial fructose concentrations^{19,20}. We therefore next assessed whether glucose might allow fructose to better support the proliferation of cancer cells. We found that the addition of even supraphysiological levels of fructose to glucose-containing media did not increase cancer cell proliferation in our experiments (Extended Data Fig. 4a–l). Fructose also had no effect on glucose metabolism, as the fate of [$U\text{-}^{13}\text{C}$]glucose was unaffected by the presence of fructose (Extended Data Fig. 4m). These findings demonstrate that the contribution of fructose to metabolism is undetectable in the presence of glucose, with [$U\text{-}^{13}\text{C}$]glucose labelling not being diluted by unlabelled fructose. Furthermore, although additional experiments showed that the polyol pathway is active in our cells, we determined that the fructose that it produces does not contribute to proliferation (Fig. 1l,m, Supplementary Note 3 and Extended Data Figs. 5 and 6a–f).

KHK-C is absent in cancer cell lines

Our isotope tracer results showed a 20-fold reduction in the ^{13}C -labelling percentage of M+3 lactate (representing a molecule with three ^{13}C labels) from [$U\text{-}^{13}\text{C}$]fructose as compared with [$U\text{-}^{13}\text{C}$]glucose, revealing that fructose metabolism is minimal in the cells that we tested. Entry of fructose into central carbon metabolism occurs through one of two enzymes: Keto hexokinase (KHK) or hexokinase (Fig. 2a). We sought to determine whether the minimal amount of metabolism observed was a product of KHK or hexokinase activity (Fig. 2a). This required establishing a LC method that resolves hexose phosphates, such as fructose 6-phosphate and fructose 1-phosphate (Extended Data Fig. 6g), which will both be present in cells when KHK is active. We determined that the level of fructose 1-phosphate was low in transformed cells, but it was ^{13}C -labelled from 5 mM [$U\text{-}^{13}\text{C}$]fructose. Measurement of ^{13}C -labelled fructose 1-phosphate suggests that endogenous and exogenous sources of fructose are phosphorylated by low levels of KHK activity in cancer cells (Fig. 2b and Extended Data Fig. 6h–m).

Note that there are two known isoforms of KHK, KHK-A and KHK-C. In non-neoplastic tissues, KHK-C is the isoform responsible for efficient metabolism of fructose. By contrast, the KHK-A isoform does not readily metabolize fructose, having a high k_m for fructose^{21–24}. Most tissues of the body express a low level of KHK-A. Only the liver, kidneys and small intestines express high amounts of KHK-C^{21,22}. Although KHK isoform expression has been studied for normal tissues, little is known about KHK isoform expression in tumours. Given that the production of fructose 1-phosphate is not specific to the activity of one isoform, we assayed the levels of KHK-A and KHK-C directly in multiple cancer cell lines. None of the cell lines that we evaluated expressed KHK-C in either normoxia or hypoxia (Fig. 2c), a condition that has been reported to induce KHK-C expression in naked mole rats and human cardiomyocytes^{23,25}. On the other hand, all cell lines expressed KHK-A (Fig. 2d). These data indicate that some KHK-A activity leads to a small level of intracellular fructose 1-phosphate (Fig. 2b), but that this activity is insufficient to enable extensive metabolism of fructose. Moreover, none of the cell lines expressed aldolase B (Extended Data Fig. 7a), which is necessary to feed fructose 1-phosphate into glycolysis (Fig. 2a). We determined that the minimal amount of labels entering central carbon metabolism from [$U\text{-}^{13}\text{C}$]fructose was a result of hexokinase, which cannot efficiently use fructose as a substrate (Supplementary Note 4 and Extended Data Fig. 7b,c). While KHK and aldolase B expression might be influenced by fructose exposure, the FBS that we used to culture cells did contain high concentrations of fructose (Supplementary Note 5 and Extended Data Fig. 7d). Moreover, we determined that the relative expression of total KHK is decreased in proliferating fibroblasts compared with quiescent fibroblasts (Extended Data Fig. 7e,f), suggesting that KHK may be downregulated during proliferation in some growth models. Notably, fructose was also not extensively metabolized in tumours isolated from mice administered dietary fructose (Supplementary Note 6 and Extended Data Fig. 7g).

PF-06835919 does not alter proliferation

To evaluate whether the small amount of KHK-A activity observed in cancer cells contributes to proliferative metabolism, we used a KHK inhibitor, PF-06835919, which was recently used in clinical trials for fatty liver disease²⁶. PF-06835919 inhibits both isoforms of KHK²⁶. We administered PF-06835919 to CaSki cells at doses up to 250 μM and observed no changes in cell proliferation (Extended Data Fig. 7h). At 30 μM , fructose 1-phosphate production in CaSki cells was undetected (Extended Data Fig. 7i). These data suggest that KHK-A production of fructose 1-phosphate is not important for cell proliferation. Administration of PF-06835919 up to 250 μM did not reduce M+3 labelling of lactate from [$U\text{-}^{13}\text{C}$]fructose, supporting that

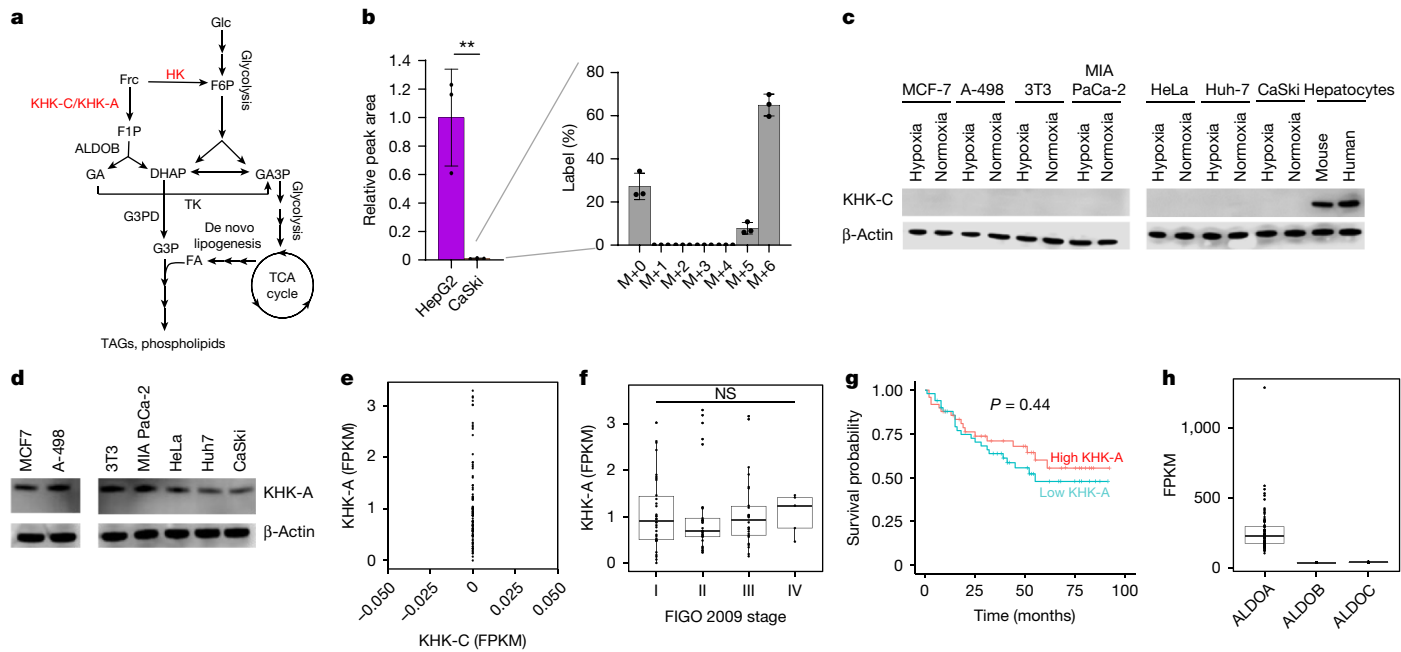


Fig. 2 | Transformed cells express KHK-A but not KHK-C. **a**, Schematic of fructose metabolism through hexokinase, KHK-C and KHK-A. F6P, fructose 6-phosphate; HK, hexokinase; F1P, fructose 1-phosphate; ALDOB, aldolase B; GA, glyceraldehyde; DHAP, dihydroxyacetone phosphate; GA3P, glyceraldehyde 3-phosphate; TK, triokinase; G3P, glycerol 3-phosphate; G3PD, glycerol 3-phosphate dehydrogenase; FA, fatty acid; TCA, tricarboxylic acid; TAG, triacylglycerol. **b**, Relative peak area of M+6 fructose 1-phosphate in CaSki cells ($n=3$) compared with HepG2 hepatocytes ($n=3$) administered 5 mM [^{13}C]fructose for 4 h. The pool of labelled fructose 1-phosphate is orders of magnitude larger in HepG2 hepatocytes, but the inset shows that fructose 1-phosphate is ^{13}C -labelled in CaSki cells after 4 h of being cultured with 5 mM [^{13}C]fructose ($n=3$). **c**, Western blot analysis of KHK-C from the indicated cell lines or primary cells. **d**, Western blot analysis of KHK-A from the indicated

cell lines. For **e–h**, data are from 99 patients treated at Washington University School of Medicine. **e**, The relative expression levels of KHK-A and KHK-C from patient cervical tumours. **f**, Patient cervical tumour stages and KHK-A isoform expression. **g**, Kaplan-Meier plot of the overall survival rate of patients expressing high levels of KHK-A or low levels of KHK-A. **h**, The relative expression levels of ALDOA, ALDOB and ALDOC from patient cervical tumours. Data in **c** and **d** are representative of two experiments. All other experiments were performed once. *P* values were determined using two-sided *t*-tests (**b**) and ordinary one-way ANOVA with Tukey's multiple-comparisons test (**f**). Survival curves were generated using a log-rank test (**g**). For **b**, data are mean \pm s.d. For the box plots in **f** and **h**, the box limits extend from the 25th to 75th percentiles, the centre line shows the median and the whiskers (**f**) extend to the largest and smallest values up to 1.5 \times the interquartile range.

the minimal amount of labelling in central carbon metabolism from [^{13}C]fructose is not due to KHK-A activity (Extended Data Fig. 7j) but, rather, hexokinase activity (Extended Data Fig. 7b,c and Supplementary Note 4). Analysis of tumours from patients with cervical cancer revealed that the levels of KHK-A and KHK-C in humans are consistent with our cell-culture results (Fig. 2e–h, Supplementary Note 7 and Extended Data Fig. 7k)

Hepatocytes transform fructose into nutrients

Given that cancer cells cannot efficiently use fructose carbon directly, we hypothesized that fructose promotes tumour growth through metabolite transfer from KHK-C expressing tissues such as the liver. We found that isolated primary mouse hepatocytes readily incorporated ^{13}C -label into their metabolome after being administered [^{13}C]fructose. In fact, the amount of ^{13}C -labelled lactate excreted was significantly higher when primary hepatocytes were provided with 5 mM [^{13}C]fructose compared to when they were provided with 5 mM [^{13}C]glucose (Fig. 3a).

To model whether the liver can convert fructose into useable nutrients for distal cancer cells, we used a Transwell system to co-culture cancer cells with mouse primary hepatocytes. We used CaSki cells as a representative cell line that lacked KHK-C and had low expression of KHK-A. As a control, the same setup was used with CaSki cells in both wells (Fig. 3b). First, we cultured cells in DMEM with 10 mM fructose as the only sugar source. When CaSki cells were co-cultured with hepatocytes, their proliferation rate increased several fold compared with the control experiment (Fig. 3c). The increased proliferation effect

of fructose was inhibited by administration of PF-06835919 (Fig. 3c). The data reveal that fructose metabolism in KHK-C expressing cells, such as hepatocytes, can support proliferation of distal cancer cells. We suspected that hepatocytes were transforming fructose carbons into nutrients that cancer cells could use to promote their proliferation. To evaluate which nutrients might be contributing to proliferation, we used LC-MS-based metabolomics to first assess which lipid metabolites were being excreted by hepatocytes and consumed by CaSki cells. We created hepatocyte-conditioned medium (hepatocyte CM) by incubating hepatocytes in medium with fructose as the only carbohydrate source for 24 h (Fig. 3d). The hepatocyte CM was then transferred to CaSki cells for 24 h, forming the CaSki-conditioned medium (CaSki CM) (Fig. 3d). A comparison of the fresh medium to the hepatocyte CM revealed which lipid metabolites were being released by hepatocytes after incubation in fructose. A comparison of the hepatocyte CM to the CaSki CM revealed which lipid metabolites released by hepatocytes were being consumed by CaSki cells. Out of more than 300 distinct lipid species that we profiled, only 21 showed a statistically significant change among all three of our sample classes (Fig. 3e). Most of the altered lipids were either triacylglycerols or unsaturated LPCs. While both triacylglycerols and LPCs were produced by hepatocytes cultured in fructose-enriched medium, only the LPCs were avidly depleted by CaSki cells (Fig. 3e). Hepatocytes have been reported to synthesize and release LPCs^{27–30}. Our data show that metabolism of fructose by hepatocytes can support this process, as LPCs were significantly ^{13}C -labelled within hepatocytes that were given [^{13}C]fructose (Fig. 3f). We performed a similar analysis for polar metabolites (Supplementary Note 8 and Extended Data Fig. 8a–c).

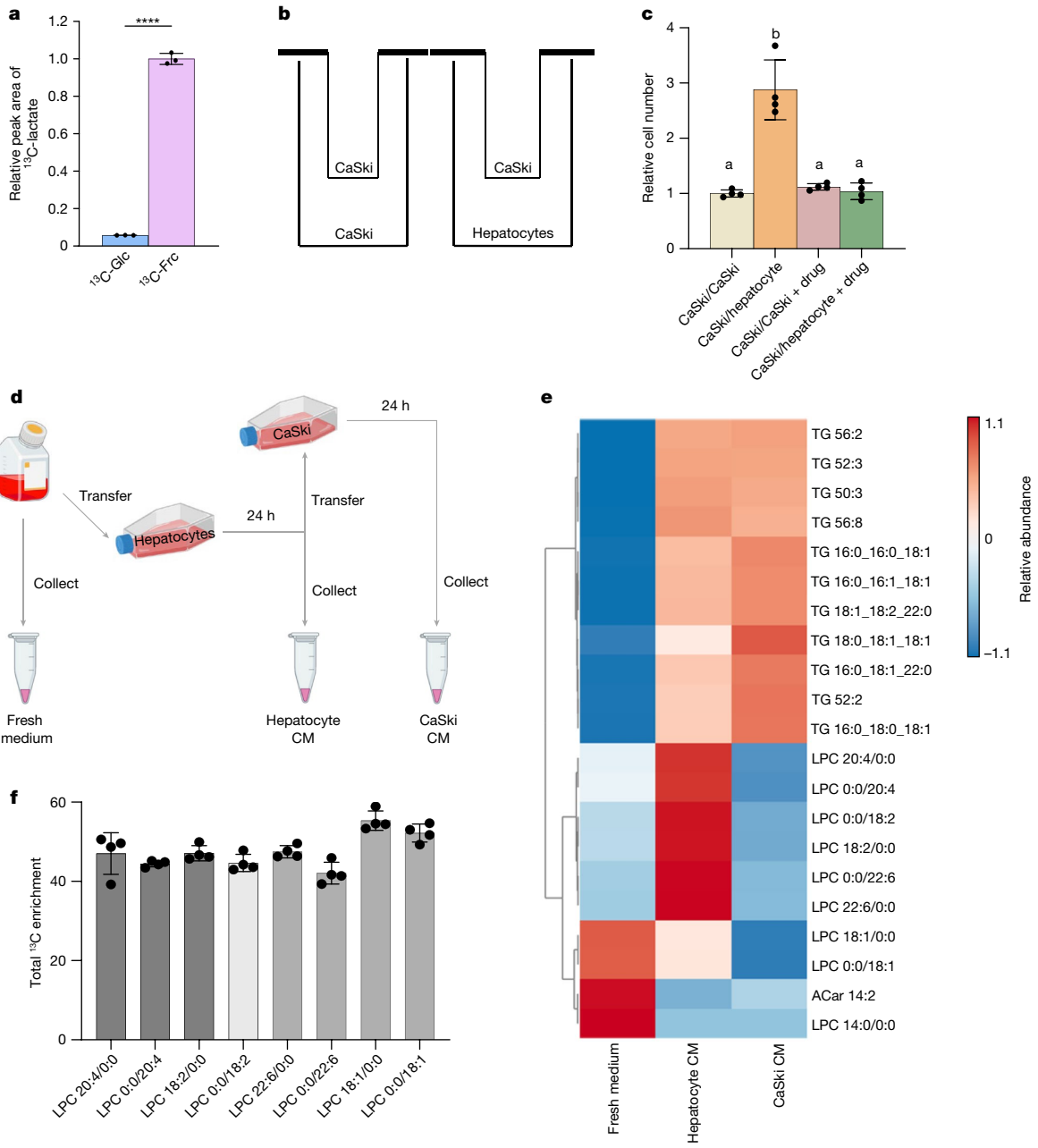


Fig. 3 | Hepatocytes transform fructose into other nutrients that support cancer cell proliferation. **a**, The relative pool size of ^{13}C -labelled lactate ($\text{M}+3$) from the medium after administering 5 mM [U^{13}C]glucose (^{13}C -Glc, $n=3$) or 5 mM [U^{13}C]fructose (^{13}C -Frc, $n=3$) to primary mouse hepatocytes for 4 h. **b**, Schematic of the Transwell co-culture experiment for CaSki + CaSki (control) or CaSki + hepatocytes. **c**, The relative number of CaSki cells in the indicated co-culture conditions treated with or without PF-06835919 (drug). $n=4$ per condition. **d**, Schematic of the generation of hepatocyte CM, CaSki CM and fresh medium for lipid analysis. Fresh medium contained 10 mM fructose as the only carbohydrate source. The image was created using BioRender. **e**, Heat map of the significant metabolite pool-size differences among the experimental

conditions outlined in **d**: fresh medium ($n=3$), hepatocyte CM ($n=6$) and CaSki CM ($n=4$). Red indicates a larger pool size. Blue indicates a smaller pool size. aCar, acylcarnitine; TG, triacylglycerol. **f**, Total ^{13}C -labelling of LPCs from primary mouse hepatocytes ($n=4$) administered 10 mM [U^{13}C] fructose. All experiments in this figure were performed once. P values were determined using two-sided t -tests (**a**) and ordinary one-way ANOVA with Tukey's multiple-comparisons test (**c**). In **c**, conditions with the same letter above the bar have no significant difference, and bars with different letters have $P < 0.05$. For **e**, significant metabolites were determined using one-way ANOVA (FDR < 0.05). For **a**, **c**, and **f**, data are mean \pm s.d.

Fructolytic tissues fuel tumour growth

On the basis of the findings of our in vitro experiments, we surmised that the effect of fructose on tumour growth in vivo was not a result of cancer cells directly using fructose but, rather, a consequence of fructose first being converted into other nutrients by fructolytic tissues expressing KHK-C and aldolase B. To compare tumour metabolism of fructose to whole-body metabolism of fructose in vivo, nude mice

bearing CaSki subcutaneous tumours were administered a one-to-one mixture of unlabelled glucose to [U^{13}C]fructose. Alternatively, mice were administered a one-to-one mixture of [U^{13}C]glucose to unlabelled fructose. First, we directly injected each mixture into the tumours of different mice. After 20 min, the tumours were collected and analysed by metabolomics for isotopic labelling. Similar to our results from cell culture, we observed extensive use of the glucose label but only minimal use of the fructose label as represented by lactate labelling (Fig. 4a).

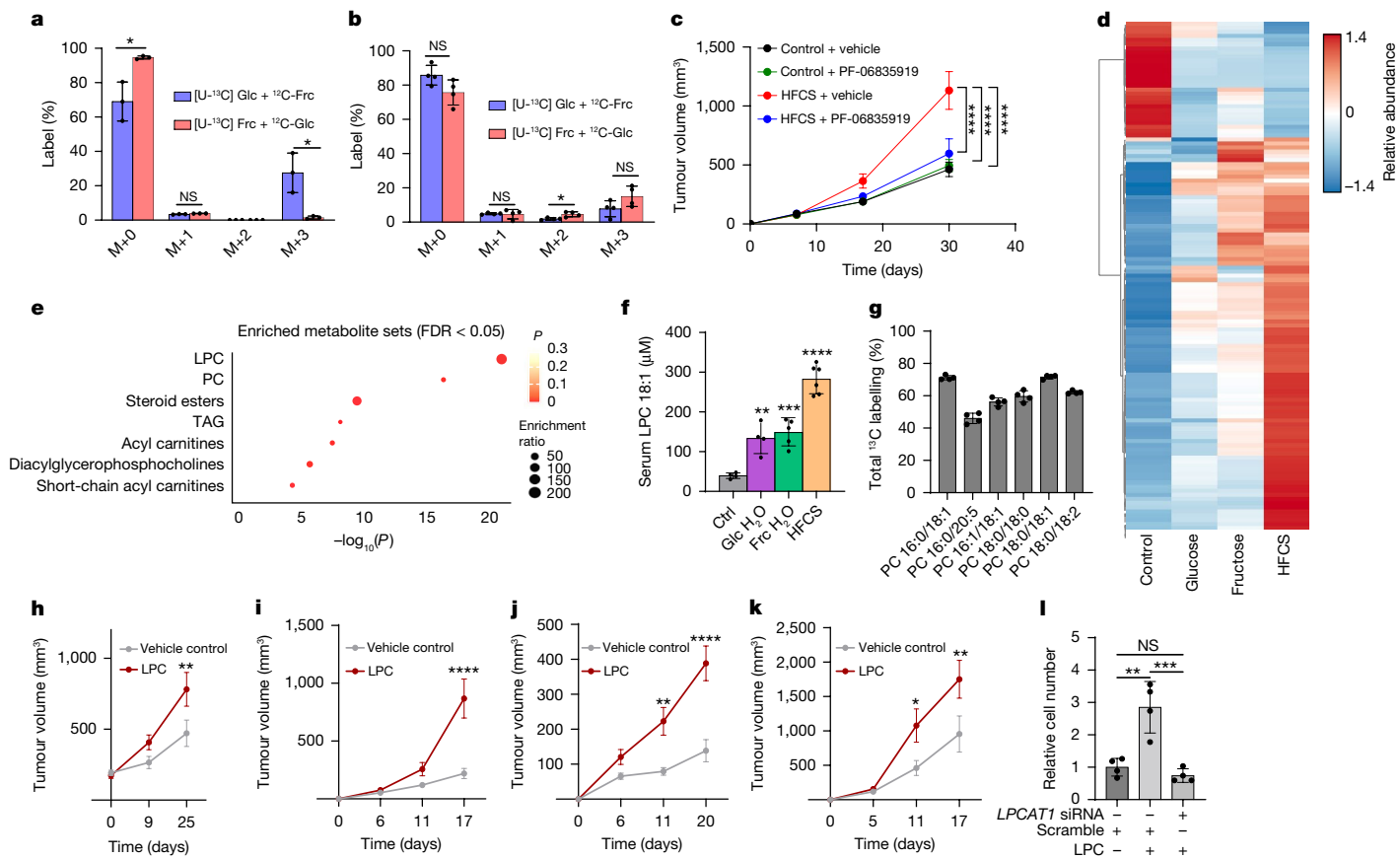


Fig. 4 | Organismal metabolism of fructose drives tumour growth. **a, b**, The isotopologue distribution for lactate from CaSki xenografts after introduction of 1:1 [^{13}C]glucose: ^{12}C -fructose or 1:1 [^{13}C]fructose: ^{12}C -glucose through direct intratumoural injection ($n = 3$ for each tracer) (**a**) or oral gavage ($n = 4$ for each tracer), ^{12}C -fructose (^{12}C -Frc) and ^{12}C -glucose (^{12}C -Glc) indicates unlabelled fructose and glucose, respectively (**b**). **c**, Tumour outgrowth of E6/E7-expressing TC-1 subcutaneous tumours after administration of PF-06835919 ($n = 6$ each drug condition) or vehicle ($n = 8$ each vehicle condition) to mice on normal water (control) or 20% HFCS water. **d**, Heat map of significant serum lipids from C57BL/6 mice on normal water ($n = 4$), 10% glucose water ($n = 4$), 10% fructose water ($n = 5$) or 20% HFCS water ($n = 6$) for 6 weeks. **e**, Metabolite set enrichment analyses of mice on normal water ($n = 4$) or 20% HFCS water ($n = 6$). The significant lipid classes increased in the 20% HFCS condition are shown. **f**, Quantification of LPC 18:1 from the serum of mice under the same conditions as in **d**. **g**, Total ^{13}C labelling, corrected for natural ^{13}C abundance, of various PCs from

E6/E7-expressing TC-1 subcutaneous tumours in mice ($n = 4$) on 5% [^{13}C] fructose water for 120 h. **h–k**, Tumour outgrowth from mice bearing CaSki (**h**), TC-1 (**i**), E0771 (**j**), or C57BL/6 melanoma (**k**). Animals were administered 80 mg per kg LPC 18:1 ($n = 7$ –8) or vehicle ($n = 7$). Mice bearing CaSki tumours were administered 80 mg per kg LPC extract from soybean ($n = 13$) or a vehicle injection ($n = 12$). **l**, Relative cell number after administering *LPCAT1* siRNA or scrambled control siRNA with or without 25 μM LPC 18:1 as indicated ($n = 4$). Data in **l** are representative of two experiments. All other experiments were performed once. *P* values were determined using multiple unpaired *t*-tests (**a** and **b**), ordinary one-way ANOVA with Tukey's multiple-comparisons test of AUC (**c**) or relative cell number (**l**), ordinary one-way ANOVA with Dunnett's multiple-comparisons test (**f**) or two-way ANOVA with Šidák's multiple-comparisons test (**h–k**). In **d**, only significant metabolites as determined by using a one-way ANOVA (FDR < 0.05) are shown. $P < 0.05$. Data are mean \pm s.e.m. (**c** and **h–k**) and mean \pm s.d. (**a**, **b**, **f**, **g** and **l**).

In a second experiment, we administered each mixture of glucose and fructose to mice by oral gavage. In contrast to direct intratumoural injection, oral gavage resulted in similar labelling of tumour metabolites such as lactate from each labelled tracer (Fig. 4b). These data indicate that, although fructose is not used by the tumour directly, the fructose carbons can be transformed into other metabolites by fructolytic tissues to feed the tumour.

Next, we evaluated the effect of systemic KHK-C inhibition on tumour growth. We already established that the KHK inhibitor PF-06835919 had no direct effect on cancer cell proliferation in vitro (Extended Data Fig. 7h). Additional experiments revealed that intraperitoneal (i.p.) administration of increasing concentrations of PF-06835919 resulted in a dose-dependent increase in mouse serum fructose, suggesting that systemic use of fructose decreased after administration of the inhibitor (Extended Data Fig. 8d). At a drug dose of 50 mg per kg, we also found that label from a large bolus of 1.5 g per kg [^{13}C]fructose was not readily used, as revealed by postprandial labelling in serum glucose (Extended Data Fig. 8e). Note that PF-06835919 was still

detected in the serum 25 h after a single 50 mg per kg dose (Extended Data Fig. 8f). Accordingly, we administered a daily 50 mg per kg dose of PF-06835919 to mice on a control diet. As expected, the drug had no effect on tumour growth (Fig. 4c and Extended Data Fig. 8g). Administration of the drug to mice on a high-fructose diet or supplemented with HFCS, however, significantly decreased tumour growth (Fig. 4c and Extended Data Fig. 8g). Similar results were obtained from zebrafish (Supplementary Note 9 and Extended Data Fig. 9). Collectively, these data show that, although fructose carbon cannot be readily used by the tumour directly, tumour growth can still be mediated by KHK-C-dependent transformation of fructose into other nutrients by fructolytic tissues.

Dietary fructose increases serum lipids and LPCs

We wished to identify representative fructose-derived nutrients produced by fructolytic tissues that could fuel tumour growth *in vivo*. Although our *in vitro* results yielded glucose and aspartate as potential

leads (Supplementary Note 8), the levels of circulating glucose and aspartate in our animals did not increase after high-fructose feeding (Extended Data Figs. 1e,f and 10a–c). We therefore turned our attention to LPCs. To test whether dietary fructose increases the availability of circulating LPCs, we used LC–MS to profile lipid metabolites from the serum of mice on high-sugar diets. For a control, mice were given regular facility water and fed a diet resembling normal chow but without any fructose or free sugars. Animals on high-sugar diets were fed the same chow but supplemented with 10% glucose water, 10% fructose water or 20% HFCS water. A comparative analysis of the serum between groups revealed 128 lipid metabolites that had statistically significant changes among all four conditions (Fig. 4d and Supplementary Table 2). Some lipids were decreased with sugar supplementation, many of which contained essential fatty acids. This most likely reflects decreased chow consumption by the mice in response to high-sugar supplementation. Many other lipid species were increased after sugar supplementation, with the HFCS condition showing the greatest elevation of lipid levels. Indeed, after fructose supplementation, de novo lipogenesis was increased in a KHK-dependent manner (Supplementary Note 10 and Extended Data Fig. 10d–i).

Metabolite set enrichment analyses of serum fasting lipids revealed that LPCs were more highly enriched ($P < 10^{-15}$) than any other lipid class in mice supplemented with HFCS compared to control conditions (Fig. 4e). We assessed the top five lipids that had the largest changes among all four conditions in terms of P value and false-discovery rate (FDR; Fig. 4d), and we found that four were LPCs. The four LPCs contained either 16:1 or 18:1 acyl chains in either the sn-1 or sn-2 positions (Extended Data Fig. 11a). Of these LPCs, LPCs containing 18:1 are present at the highest concentration in the serum³¹ and we therefore predicted that LPC 18:1 could be an important nutrient for cancer cells.

To further evaluate the potential contribution of fructose-derived LPC 18:1 to tumour growth, we quantified its concentration in the fasting serum of mice on each diet. We found that diets supplemented with glucose or fructose both resulted in similar increases in LPC 18:1 availability. Supplementing diets with HFCS resulted in even higher LPC 18:1 serum levels, most likely reflecting the additive effects of both glucose and fructose (Fig. 4f). To confirm that LPC 18:1 in the serum was being derived from fructose, we provided C57BL/6 mice access to drinking water enriched with 5% [$U\text{-}^{13}\text{C}$]fructose for 60 h. Subsequent analysis of the serum for LPC 18:1 revealed labelling, demonstrating that LPC 18:1 can be derived from fructose carbon (Extended Data Fig. 11b). A more detailed analysis revealed that fructose carbons can contribute to both the glycerol backbone and fatty acyl chain of LPCs (Supplementary Note 11 and Extended Data Fig. 11c,d).

Tumours convert LPCs to PCs

As further support that tumours deplete LPC 18:1 from the serum, we compared its concentration in the serum of mice to its concentration in the tumour interstitial fluid (TIF). We found that LPC 18:1 levels in the TIF were decreased by 6–20-fold compared with matched serum of animals bearing *Braf^{V600E}Pten^{-/-}* melanoma, E0771, TC-1 and CaSki tumours (Extended Data Fig. 11e). These data suggest depletion of LPC 18:1 by the tumour (Extended Data Fig. 11e).

To characterize the metabolic fates of LPC 18:1 within cancer cells, we administered 20 μM deuterium-labelled LPC 18:1 to CaSki cells for 3 days, refreshing the medium every 24 h. The tracer of LPC 18:1 that we used contained seven deuterium labels on the fatty acyl chain. In treated cells, we found that over 70% of the 18:1-containing phosphatidylcholines (PCs) that we analysed were enriched with seven deuterium labels, indicating that a substantial portion of cellular PCs are derived from exogenous LPC (Extended Data Fig. 11f). To demonstrate that LPC 18:1 is used by cancer cells to produce PCs *in vivo*, we subcutaneously introduced the same LPC 18:1 tracer to C57BL/6 mice and showed that deuterium labels are incorporated into PC species containing 18:1

acyl side chains within tumours (Extended Data Fig. 11g). As further evidence that fructose supports the production of PCs in tumours, we provided C57BL/6 mice with access to 5% [$U\text{-}^{13}\text{C}$]fructose water for 120 h. We observed ^{13}C -enrichment of PCs in TC-1 tumours, with more than 50% of some species containing label derived from fructose (Fig. 4g). We also observed significant enrichment in intratumoural LPCs (Extended Data Fig. 11h). These data suggest that a major metabolic fate of fructose-derived lipids such as LPC 18:1 within cancer cells is phospholipids, which are essential to produce membranes during proliferation.

We wanted to confirm that access to LPC 18:1 promotes cancer cell proliferation and increases tumour growth. To that end, we first cultured *Braf^{V600E}Pten^{-/-}* melanoma, E0771, TC-1 and CaSki cells with increasing concentrations of LPC 18:1 (Extended Data Fig. 12a–d). In all cases, we found that higher LPC 18:1 levels led to increased proliferation rates *in vitro*. Second, to assess the impact of LPC 18:1 availability on tumour growth *in vivo*, we administered 80 mg per kg LPC 18:1 (or an LPC extract) to mice bearing *Braf^{V600E}Pten^{-/-}* melanoma, E0771, TC-1 or CaSki subcutaneous tumours. The 80 mg per kg dose of LPC 18:1, which was given twice daily through subcutaneous injection, was sufficient to elevate serum LPC 18:1 levels for several hours (Extended Data Fig. 12e). Administration of LPC 18:1 increased the growth of all of the tumours tested (Fig. 4h–k). According to this mechanism, we speculated that the KHK inhibitor PF-06835919 would decrease the LPC 18:1 levels in the serum. As predicted, daily i.p. administration of 50 mg per kg PF-06835919 to C57BL/6 mice for 7 days on a diet supplemented with 10% fructose water restored LPC 18:1 serum levels to those observed in mice on a control diet (Extended Data Fig. 12f).

LPCs can be converted into PCs through a one-step reaction catalysed by lysophosphatidylcholine acyltransferases (LPCATs)³². Of the four isoforms, LPCAT1 was determined to have the highest expression in CaSki cells (Extended Data Fig. 12g). Previous work already demonstrated that LPCAT1 is overexpressed in multiple cancers and contributes to disease progression^{33–35}. We therefore focused on LPCAT1 in CaSki cells. We found that knocking down *Lpcat1* rescued LPC-enhanced cell proliferation (Fig. 4l and Extended Data Fig. 12h), suggesting an important role of exogenous LPCs for membrane formation. Together, these data support a model in which increased levels of circulating LPCs derived from fructose promote tumour growth (Extended Data Fig. 12i).

Discussion

Here we evaluated whether a panel of transformed cells could use fructose as a fuel in monoculture over the time scale of postprandial fructose exposure. Even when the cells were exposed to supraphysiological concentrations of fructose, we found that fructose could not be metabolized efficiently because the cells did not express KHK-C or aldolase B. Notably, transformed cell lines from fructolytic tissues also did not express fructolytic enzymes (Fig. 2c and Extended Data Fig. 7a), which is consistent with other reports that hepatocellular carcinoma and renal cell carcinoma tumours stop expressing KHK-C^{36,37}. In contrast to our *in vitro* results, we did observe that fructose promotes the growth of orthotopic tumours derived from the same cell lines. We determined that the mechanism by which fructose promoted the growth of tumours in the skin, breast and cervix was not cell autonomous but was instead a consequence of its metabolism in fructolytic tissues, which increases the levels of circulating lipids such as LPCs. We focused on tumours from three types of non-fructolytic tissues here, but we cannot rule out the possibility that other tumours in different peripheral locations have the ability to use fructose directly as a fuel. A mechanism in which fructose promotes tumour growth directly and a mechanism whereby fructose promotes tumour growth indirectly are not mutually exclusive. For some tumours, both processes might contribute to disease progression.

Although the effect of high-fructose diets on phospholipids has received less attention than triacylglycerols and sterols^{13,19,38,39}, increased levels of LPCs in the serum have been linked to high-fructose consumption in humans⁴⁰. Unsaturated LPCs in the serum primarily originate from the liver^{27–30}. Mice administered high-fructose diets did not gain weight or develop insulin resistance in our study, but we did observe dyslipidaemia. The most dysregulated lipids in the serum were LPCs, with fasting levels of LPC 18:1 increasing more than sevenfold in mice given HFCS for several weeks compared with mice on a control diet (Fig. 4f). LPC 18:1 levels were also depleted in the TIF of animals bearing tumours, suggesting use by tumours (Extended Data Fig. 11e). Indeed, other studies have reported decreased levels of circulating LPCs in various types of human cancer, which may indicate increased turnover due to the metabolic burden of the tumour^{41–44}.

To proliferate, cancer cells must form new membranes. The required membrane precursors could be made de novo; however, lipid synthesis requires a considerable amount of energy. Increasing evidence suggests that proliferating cancer cells therefore scavenge lipids from their environment. The focus of previous work has largely been on the consumption of free fatty acids, but the major phospholipids in cellular membranes are PCs^{45,46}. Although consumption of exogenous PCs would be most efficient, circulating LPCs are more structurally similar to PCs than free fatty acids and they might be more accessible than PCs⁴⁷. We conclude that one way in which high levels of fructose consumption promote tumour growth in our models is by increasing the availability of LPCs to cancer cells. We suggest that future studies examine the possibility of LPC use by tumours as a potential therapeutic target.

Online content

Any methods, additional references, Nature Portfolio reporting summaries, source data, extended data, supplementary information, acknowledgements, peer review information; details of author contributions and competing interests; and statements of data and code availability are available at <https://doi.org/10.1038/s41586-024-08258-3>.

- Vos, M. B., Kimmons, J. E., Gillespie, C., Welsh, J. & Blank, H. M. Dietary fructose consumption among US children and adults: The Third National Health and Nutrition Examination Survey CME. *Medscape Gen. Med.* **10**, 160 (2008).
- Nakagawa, T. et al. Fructose contributes to the Warburg effect for cancer growth. *Cancer Metab.* **8**, 16 (2020).
- Kanarek, N., Petrova, B. & Sabatini, D. M. Dietary modifications for enhanced cancer therapy. *Nature* **579**, 507–517 (2020).
- Jeong, S. et al. High fructose drives the serine synthesis pathway in acute myeloid leukemic cells. *Cell Metab.* **33**, 145–159.e6 (2021).
- Liu, H. et al. Fructose induces transketolase flux to promote pancreatic cancer growth. *Cancer Res.* **70**, 6368–6376 (2010).
- Goncalves, M. D. et al. High-fructose corn syrup enhances intestinal tumor growth in mice. *Science* **363**, 1345–1349 (2019).
- Bu, P. et al. Aldolase B-mediated fructose metabolism drives metabolic reprogramming of colon cancer liver metastasis. *Cell Metab.* **27**, 1249–1262 (2018).
- Chen, W. L. et al. GLUT5-mediated fructose utilization drives lung cancer growth by stimulating fatty acid synthesis and AMPK/mTORC1 signaling. *JCI Insight* **5**, e131596 (2020).
- Godoy, A. et al. Differential subcellular distribution of glucose transporters GLUT1–6 and GLUT9 in human cancer: ultrastructural localization of GLUT1 and GLUT5 in breast tumor tissues. *J. Cell. Physiol.* **207**, 614–627 (2006).
- Liang, R. J. et al. GLUT5 (SLC2A5) enables fructose-mediated proliferation independent of ketohexokinase. *Cancer Metab.* **9**, 12 (2021).
- Douard, V. & Ferraris, R. P. The role of fructose transporters in diseases linked to excessive fructose intake. *J. Physiol.* **591**, 401 (2013).
- Francey, C. et al. The extra-splanchnic fructose escape after ingestion of a fructose–glucose drink: an exploratory study in healthy humans using a dual fructose isotope method. *Clin. Nutr. ESPEN* **29**, 125–132 (2019).
- Herman, M. A. & Birnbaum, M. J. Molecular aspects of fructose metabolism and metabolic disease. *Cell Metab.* **33**, 2329–2354 (2021).
- Jang, C. et al. The small intestine converts dietary fructose into glucose and organic acids. *Cell Metab.* **27**, 351–361.e3 (2018).
- Patton, E. E. et al. BRAF mutations are sufficient to promote nevi formation and cooperate with p53 in the genesis of melanoma. *Curr. Biol.* **15**, 249–254 (2005).
- Febbraio, M. A. & Karin, M. ‘Sweet death’: fructose as a metabolic toxin that targets the gut–liver axis. *Cell Metab.* **33**, 2316–2328 (2021).
- Bray, G. A., Nielsen, S. J. & Popkin, B. M. Consumption of high-fructose corn syrup in beverages may play a role in the epidemic of obesity. *Am. J. Clin. Nutr.* **79**, 537–580 (2004).
- Taskinen, M. R., Packard, C. J. & Borén, J. Dietary fructose and the metabolic syndrome. *Nutrients* **11**, 1987 (2019).
- Sun, S. Z. & Empie, M. W. Fructose metabolism in humans—what isotopic tracer studies tell us. *Nutr. Metab.* **9**, 89 (2012).
- Chong, M. F. F., Fielding, B. A. & Frayn, K. N. Mechanisms for the acute effect of fructose on postprandial lipemia. *Am. J. Clin. Nutr.* **85**, 1511–1520 (2007).
- Diggle, C. P. et al. Ketohexokinase: expression and localization of the principal fructose-metabolizing enzyme. *J. Histochem. Cytochem.* **57**, 763–774 (2009).
- Ishimoto, T. et al. Opposing effects of fructokinase C and A isoforms on fructose-induced metabolic syndrome in mice. *Proc. Natl. Acad. Sci. USA* **109**, 4320–4325 (2012).
- Mirtschink, P. et al. HIF-driven SF3B1 induces KHK-C to enforce fructolysis and heart disease. *Nature* **522**, 444–449 (2015).
- Asipi, A., Hayward, B. E., O'Reilly, J. & Bonthon, D. T. Properties of normal and mutant recombinant human ketohexokinases and implications for the pathogenesis of essential fructosuria. *Diabetes* **52**, 2426–2432 (2003).
- Park, T. J. et al. Fructose-driven glycolysis supports anoxia resistance in the naked mole-rat. *Science* **356**, 307–311 (2017).
- Futatsugi, K. et al. Discovery of PF-06835919: a potent inhibitor of ketohexokinase (khk) for the treatment of metabolic disorders driven by the overconsumption of fructose. *J. Med. Chem.* **63**, 13546–13560 (2020).
- Sekas, G., Patton, G. M., Lincoln, E. C. & Robins, S. J. Origin of plasma lysophosphatidylcholine: Evidence for direct hepatic secretion in the rat. *J. Lab. Clin. Med.* **105**, 185–189 (1985).
- Graham, A., Zammit, V. A. & Brindley, D. N. Fatty acid specificity for the synthesis of triacylglycerol and phosphatidylcholine and for the secretion of very-low-density lipoproteins and lysophosphatidylcholine by cultures of rat hepatocytes. *Biochem. J.* **249**, 727–733 (1988).
- Baisted, D. J., Robinson, B. S. & Vancet, D. E. Albumin stimulates the release of lysophosphatidylcholine from cultured rat hepatocytes. *Biochem. J.* **253**, 693–701 (1988).
- Graham, A. et al. Factors regulating the secretion of lysophosphatidylcholine by rat hepatocytes compared with the synthesis and secretion of phosphatidylcholine and triacylglycerol. Effects of albumin, cycloheximide, verapamil, EGTA and chlorpromazine. *Biochem. J.* **253**, 687–692 (1988).
- Ojala, P. J., Hirvonen, T. E., Hermansson, M., Somerharju, P. & Parkkinen, J. Acyl chain-dependent effect of lysophosphatidylcholine on human neutrophils. *J. Leukoc. Biol.* **82**, 1501–1509 (2007).
- Law, S. H. et al. An updated review of lysophosphatidylcholine metabolism in human diseases. *Int. J. Mol. Sci.* **20**, 1149 (2019).
- Gao, F., Chen, J., Zhang, T. & Liu, N. LPCAT1 functions as an oncogene in cervical cancer through mediating JAK2/STAT3 signaling. *Exp. Cell. Res.* **421**, 113360 (2022).
- Bi, J. et al. Oncogene amplification in growth factor signaling pathways renders cancers dependent on membrane lipid remodeling. *Cell Metab.* **30**, 525–538 (2019).
- Mansilla, F. et al. Lysophosphatidylcholine acyltransferase 1 (LPCAT1) overexpression in human colorectal cancer. *J. Mol. Med.* **87**, 85 (2009).
- Tee, S. S. et al. Ketoheinoxinase-mediated fructose metabolism is lost in hepatocellular carcinoma and can be leveraged for metabolic imaging. *Sci. Adv.* **8**, 7985 (2022).
- Hwa, J. S. et al. The expression of ketoheinoxinase is diminished in human clear cell type of renal cell carcinoma. *Proteomics* **6**, 1077–1084 (2006).
- David Wang, D. et al. Effect of fructose on postprandial triglycerides: a systematic review and meta-analysis of controlled feeding trials. *Atherosclerosis* **232**, 125–133 (2014).
- Jang, C. et al. The small intestine shields the liver from fructose-induced steatosis. *Nat. Metab.* **2**, 586–593 (2020).
- Gonzalez-Granda, A., Damms-Machado, A., Basrai, M. & Bischoff, S. C. Changes in plasma acylcarnitine and lysophosphatidylcholine levels following a high-fructose diet: a targeted metabolomics study in healthy women. *Nutrients* **10**, 1254 (2018).
- Kuliszkiewicz-Janus, M., Tuz, M. A. & Baczyński, S. Application of 31P MRS to the analysis of phospholipid changes in plasma of patients with acute leukemia. *Biochim. Biophys. Acta* **1737**, 11–15 (2005).
- Zhao, Z. et al. Plasma lysophosphatidylcholine levels: potential biomarkers for colorectal cancer. *J. Clin. Oncol.* **25**, 2696–2701 (2007).
- Qiu, Y. et al. Mass spectrometry-based quantitative metabolomics revealed a distinct lipid profile in breast cancer patients. *Int. J. Mol. Sci.* **14**, 8047–8061 (2013).
- Süllentrop, F. et al. 31P NMR spectroscopy of blood plasma: Determination and quantification of phospholipid classes in patients with renal cell carcinoma. *NMR Biomed.* **15**, 60–68 (2002).
- Yao, C. H. et al. Exogenous fatty acids are the preferred source of membrane lipids in proliferating fibroblasts. *Cell Chem. Biol.* **23**, 483–493 (2016).
- Corn, C. K., Windham, M. A. & Rafat, M. Lipids in the tumor microenvironment: from cancer progression to treatment. *Prog. Lipid Res.* **80**, 101055 (2020).
- Kamphorst, J. J. et al. Hypoxic and Ras-transformed cells support growth by scavenging unsaturated fatty acids from lysophospholipids. *Proc. Natl. Acad. Sci. USA* **110**, 8882–8887 (2013).

Publisher's note Springer Nature remains neutral with regard to jurisdictional claims in published maps and institutional affiliations.

Springer Nature or its licensor (e.g. a society or other partner) holds exclusive rights to this article under a publishing agreement with the author(s) or other rightsholder(s); author self-archiving of the accepted manuscript version of this article is solely governed by the terms of such publishing agreement and applicable law.

© The Author(s), under exclusive licence to Springer Nature Limited 2024

Methods

Mouse studies

All mouse procedures were approved by the Washington University Institutional Animal Care and Use Committee (IACUC; 19-0930 and 22.0304). The maximum tumour volume permitted by the IACUC in our mice is 2,000 mm³. After this point, mice were euthanized. All mice used in the study were female. Athymic nude mice were purchased from Charles River Laboratory at 6–8 weeks of age. C57BL/6J mice were purchased from The Jackson Laboratory. All mice were housed under 12 h–12 h light–dark cycles at 22 °C. Diets were provided ad libitum and mice were weighed weekly. Mice were randomized to experimental conditions. Investigators were not blinded to experimental conditions.

The number of mice used in each experiment is reported in the associated figure legends. Unless otherwise noted, before the formation of xenografts, mice were started on their diet or sugar-water conditions for 3 weeks. After 3 weeks of pretreatment, CaSkI xenografts were formed by injection of 3 million cells in 1:1 DMEM:Matrigel into the left flank of female athymic nude mice. TC-1, E0771 and *Braf*^{V600E}-mutant, *Pten*-deficient mouse melanoma xenografts were formed by injection of 300,000 cells into the flank or relevant orthotopic site of C57BL/6J where indicated. The first tumour volume measurement was several days after tumour implantation. For formation of the cervical orthotopic E6/E7-expressing TC-1 tumour, C57BL/6 mice were subcutaneously injected with 3 mg of medroxyprogesterone (McKesson) on day 1 and 1 mg on day 3. On day 4, mice were injected intravaginally with 10 mg of nonoxynol-9 (Millipore-Sigma). On day 5, luciferase-positive E6/E7-expressing TC-1 cells were implanted by intravaginally injecting 250,000 cells into the cervix. Tumours were monitored with bioluminescence imaging on the IVIS Lumina III. After 2 weeks of growth, mice were euthanized and the tumour volume was assessed. For gavage of 0.5 mg per kg [U-¹³C]fructose in tumour mice versus tumour-free mice, 500,000 E6/E7-expressing TC-1 cells were subcutaneously injected into mice. Then, 2 weeks after TC-1 implantation, mice were gavaged. For subcutaneous xenografts or E0771 cells injected into the mammary fat pad, a needle was used to administer the cells to the appropriate body site. Tumour size in all models was then assessed at indicated timepoints with callipers and the volume was calculated by using the formula $V = (1/2)(L \times W^2)$, where L and W are length and width, respectively. Mice were fed a control diet (Envigo, TD.05075) or a high-fructose diet (Envigo TD.89247) ad libitum. Mice were administered sugar in their water by providing a control diet (Envigo, TD.05075) with ad libitum access to 10% fructose, 10% glucose or 20% HFCS water. The sugar ratios in the HFCS solution were 55:45 fructose:glucose. The water bottles were not added to the mouse cages until the experiment started and the mouse cage locations were fixed. Before that, water bottles were kept upright to prevent leakage. This protocol reduced the risk of spilling water and ensured that the only source of water depletion was from water consumption by animals. Signs were placed on the cages to ensure that mouse facility staff did not disturb the cage during the course of the experiment. For D₂O labelling, C57BL/6 female mice were first given access to control water, 10% fructose water or 10% fructose water with daily 50 mg per kg PF-06835919 i.p. injections for 7 days. The mice were then given access to 50% D₂O water in the same pretreatment conditions for 12 h before mice were euthanized and their livers collected for analysis by LC-MS.

All LPCs were suspended in normal saline before injection, with saline alone serving as the vehicle. In all experiments, LPC 18:1 (Avanti Polar Lipids) or an LPC extract from Glycine Max (Millipore-Sigma) was used. For tumour growth studies, mice were subcutaneously injected with 80 mg per kg of LPC twice daily. All isotopic labels were purchased from Cambridge Isotope Labs or Avanti Polar lipids. The LPC 18:1-D7 tracer was introduced subcutaneously three times at a dose of 80 mg per kg every 4 h, thereby spanning a total time of 12 h. The tracer was

administered at a distal site from TC-1 tumours. To show that tumours produced PC species from fructose, mice were given access to water containing 5% [U-¹³C]fructose for 120 h. To assess fractional carbon atom enrichment in LPCs, we used the experimental setup shown in Extended Data Fig. 11c. In brief, mice were placed on 10% [U-¹³C]fructose water for 84 h. The serum was then collected during dark hours while mice had access to food and 10% [U-¹³C]fructose water. Next, these same mice were fasted for 12 h (with access only to normal water) and serum was collected again.

Stock solutions of ¹³C-labelled nutrients were made for injection into mouse tumours by suspending 200 mg ¹³C-labelled nutrient per ml of normal saline. The amount of labelled stock solution injected into each mouse tumour was normalized by tumour volume (40 µl of stock solution/200 mm³ CaSkI tumour volume). Tumours were collected 20 min after direct intratumour injection of ¹³C label. The same stock solution of 200 mg ¹³C-labelled nutrient per ml of normal saline was used for oral gavage. When introducing ¹³C-labelled nutrients by gavage, a feeding needle was used to introduce 5 µl of labelled stock solution per g of mouse weight.

PF-06835919 was administered through i.p. injection in 10% DMSO and 10% Tween-80 in normal saline at the doses indicated. In experiments in which mice were given PF-06835919 through i.p. injection and [U-¹³C]fructose through gavage, a feeding needle was used to introduce 1.5 g of [U-¹³C]fructose stock solution per kg of mouse weight. In all isotope-tracer experiments, the mice were fasted for 4 h before the administration of label. Mouse whole-blood samples (approximately 25 µl) were collected through tail snip. Mouse xenograft tumours were collected through rapid manual dissection with a scalpel and flash-frozen in liquid nitrogen. Tissues were stored at –80 °C until extraction for LC-MS analysis.

Serum insulin and glucose were assessed in nude or C57BL/6 mice after 12 h of fasting. Glucose was measured with LC-MS. Insulin was measured by using the Ultra Sensitive Mouse Insulin ELISA Kit (Crystal Chem). Glucose tolerance tests were performed by fasting mice for 4 h, after which 1.5 g per kg glucose was administered as an oral gavage. Blood was collected from tail snips and serum glucose was quantified with LC-MS. Alanine tolerance tests were performed by fasting mice for 4 h, after which 0.5 g per kg [U-¹³C] alanine was administered as an oral gavage. Blood was collected from tail snips and serum ¹³C-glucose was quantified by using LC-MS.

TIF was isolated as previously described⁴⁸. In brief, tumours were quickly dissected from the animal, rinsed in PBS and thoroughly blotted dry. Tumours were placed onto a 20 µM filter (Cole-Parmer) on top of a conical tube and centrifuged for 10 min at 106g. TIF was collected from the bottom of the tube for subsequent analysis.

Zebrafish

All zebrafish procedures were approved by the Washington University Institutional Animal Care and Use Committee (protocol number 21-0349). The number of *Tg(mitfa:BRAF^{V600E});p53*^{−/−} fish (referred to as *BRAF/p53* fish)⁴⁹ used in each experiment is reported in the associated figure legends. Fish were reared according to standard laboratory procedures. Fish were kept in an indoor environment at a temperature of 28 ± 1 °C under a 14 h–10 h light–dark circadian cycle. Fish were euthanized with an ice bath. Euthanasia was deemed to be complete 1 min after cessation of opercular movement in an ice water slurry. Zebrafish were randomized to experimental conditions. Investigators were not blinded to experimental conditions.

To perform *in vivo* ¹³C-labelling of *BRAF/p53* fish, 50 mM of either [U-¹³C]glucose or [U-¹³C]fructose was dissolved directly into zebrafish tank water containing 3% penicillin–streptomycin (Life Technologies), 5 µg ml^{−1} kanamycin (Millipore-Sigma) and 100 µg ml^{−1} ampicillin (Millipore-Sigma) to prevent bacterial contamination. Fish were maintained at a density of 1 fish per 100 ml ¹³C-labelled water. Fish were maintained in labelled water for 30 h before euthanasia. Tumours

Article

were rapidly collected from the surface of the body, snap-frozen in liquid nitrogen and stored at -80°C until LC–MS analysis. Serum and tissues were collected as described below.

To perform the tumour regrowth assay, *BRAF/p53* zebrafish were anaesthetized in tricaine and a scalpel was used to amputate their tumours to be flush with the surface of the skin. Every fish had tumour tissue that extended beneath the surface of the skin, and this portion of the tumour remained after dissection. The fish were then randomized to each treatment condition. All water conditions had 3% penicillin-streptomycin, 5 $\mu\text{g ml}^{-1}$ kanamycin and 100 $\mu\text{g ml}^{-1}$ ampicillin antibiotics. For the fructose-treated or glucose-treated groups, fish were transferred to water containing 100 mM fructose or 100 mM glucose, respectively, in addition to antibiotics. For the control group, fish were in the same water conditions without fructose and glucose. For the fructose-treated and PF-06835919-treated group, 200 μM PF-06835919 was dissolved into water containing 100 mM fructose and antibiotics. The drug was first dissolved in DMSO to achieve a final concentration of 0.25% (v/v) in zebrafish water. DMSO alone was used as a vehicle control. The water in all conditions was changed every other day to prevent bacterial contamination. Fish were fed brine shrimp once a day in each condition. After 2 weeks in each condition, tumour regrowth was assessed by using callipers. Tumour volume above the surface of the skin was calculated by using the formula $V = (W \times L \times H) \times 0.5236$, where W , L and H are width, length and height respectively.

To administer PF-06835919 or vehicle control (DMSO) to *BRAF/p53* zebrafish labelled with [$\text{U}-^{13}\text{C}$]fructose, a 10 μl nanofil syringe (WPI) was used to inject 50 mg per kg of PF-06835919 into the fish peritoneum. PF-06835919 was dissolved in DMSO and the i.p. injection volume was 2 μl drug solution per gram zebrafish weight. Then, 1 h after i.p. injection with PF-06835919, the fish were placed into aquarium water containing 25 mM [$\text{U}-^{13}\text{C}$]fructose, 190 μM PF-06835919, 3% penicillin-streptomycin, 5 $\mu\text{g ml}^{-1}$ kanamycin and 100 $\mu\text{g ml}^{-1}$ ampicillin. Fish that were i.p. injected with vehicle were placed into the same water conditions, except without PF-06835919. After 12 h, fish in both conditions were euthanized and the serum was collected as described below.

To collect *BRAF/p53* zebrafish serum for LC–MS analysis, the following method was used⁵⁰. A simple blood collection device was constructed by forming a small hole in the bottom of a microcentrifuge tube (the holding tube) with a razor blade. The hole was approximately the diameter of the cross-section created through distal amputation of a given fish. This holding tube was then fitted into another microcentrifuge tube (the collection tube), and the connection was secured with tape. To begin the blood-collection process, fish were euthanized in ice water as described above. Fish were then removed from ice water and dried thoroughly with a kimwipe. A razor blade was used to amputate the caudal fin and some associated distal tissue by making a transverse cross section midway between the anal and caudal fin. The amputated fish were immediately placed into the holding tube (with the wound end nearest the hole). The holding tube was then placed into the collection tube, securing the connection with tape. We placed the entire collection device containing the amputated fish into a microcentrifuge and centrifuged at 1,000 rpm and 28°C for 1 min. Tissues were anatomically dissected, snap-frozen in liquid nitrogen and stored at -80°C until extraction for LC–MS analysis.

Human and zebrafish *KHK* DNA sequences were downloaded from the UCSC Genome Browser⁵¹ with Table Brower and pairwise aligned by using EMBOSS Needle⁵², then visualized in the UCSC Genome Brower to compare exon sequences and determine which zebrafish *KHK* isoforms correspond to which human *KHK* isoforms. RNA-seq reads from a total of 13 different zebrafish tissues were downloaded from the NCBI SRA archives⁵³ (SRP213938) in FASTQ format and aligned to the zebrafish reference genome (GRCz11/danRer11) by using STAR2⁵⁴. Cufflinks⁵⁵ was run to predict gene expression and isoform expression for all isoforms. The read alignments were then visualized in IGV⁵⁶ and inspected for junctions unique to each *KHK* isoform.

To administer [$\text{U}-^{13}\text{C}$]inulin, antibiotic-treated fish were pretreated for 7 days in water containing 5 $\mu\text{g ml}^{-1}$ kanamycin (Millipore-Sigma), 100 $\mu\text{g ml}^{-1}$ ampicillin (Millipore-Sigma), 250 ng ml^{-1} amphotericin B (Millipore-Sigma) and 2% penicillin–streptomycin (Millipore-Sigma). Antibiotic-treated and control fish were then fasted for 24 h, after which 1.5 g per kg of [$\text{U}-^{13}\text{C}$]inulin was administered through oral gavage by using a pipette. The fish were sacrificed 90 min later and the intestines and serum were collected for LC–MS analysis.

Preparation of mouse and zebrafish serum

Mouse and zebrafish whole-blood samples were placed on ice without anticoagulant for 20 min. The samples were subsequently centrifuged at 6,000 rpm for 10 min. The serum was then collected and stored at -80°C until extraction for LC–MS analysis.

Cell culture

Human and mouse cell lines were maintained in high-glucose DMEM (Life Technologies) containing 10% FBS (Life Technologies) and 1% penicillin–streptomycin (Life Technologies). Cell lines were cultured at 37°C and 5% CO_2 , except Zcrest C zebrafish melanoma cells, which were cultured at 28.5°C and 5% CO_2 . Hypoxic cells were cultured at 37°C , 5% CO_2 , and 1% oxygen for 3 days. HeLa cells were obtained from the Tissue Culture Support Center of Washington University in St Louis. HeLa cells are a commonly misidentified cell line as defined by the International Cell Line Authentication Committee. HeLa cells were selected for this study because they are one of the most commonly studied cervical cancer cell lines. We note that our results from HeLa cells were validated in the other cell lines used in this study. CaSki and SiHa cells were obtained from the laboratory of J. Schwarz. E6,E7-expressing TC-1 cells (often simply referred to as “TC-1” throughout the text) were obtained from the laboratory of T. C. Wu at Johns Hopkins. *Braf*^{V600E}-mutant, *Pten*-deficient mouse melanoma cells were obtained from the laboratory of G. Souroullas and were derived from the *Tyr::cre*^{ERT2}*Braf*^{V600E/+}*Pten*^{R/R} genetically engineered C57BL/6 mouse models described previously⁵⁷. A-498 cells were obtained from the laboratory of J. Hsieh. MIA PaCa-2 cells were obtained from the laboratory of W. Hawkins. Huh7 cells were obtained from the laboratory of B. Finck. Zcrest C zebrafish melanoma cells were obtained from the laboratory of C. Kaufman. E0771 (94A001) cells were obtained from CH3 BioSystems. MCF-7 (HTB-22) and 3T3-L1 (CL-173) cells were obtained from American Type Culture Collection. Cell lines were authenticated with STR profiling. Cells tested negative for mycoplasma contamination.

For all monoculture proliferation studies, cells were maintained under the indicated conditions for 3–4 days. A 10 mM concentration of fructose or glucose was used to prevent the cells from depleting the respective sugars over the timescale of the experiment. For BSA-LPC 18:1 studies, the indicated concentration of lipid was added to media comprising high-glucose DMEM and 10% dialysed FBS and 100 μM carnitine. BSA concentrations were manually adjusted to be the same in all conditions. For the co-culture study, CaSki cells and hepatocytes were maintained under the indicated conditions for 48 h. For non-polar media transfer analysis, 10 mM fructose was dissolved in glucose-free DMEM and 10% dialysed FBS with 1% penicillin–streptomycin. The media was used to culture hepatocytes, ultimately yielding hepatocyte-conditioned media. For polar media transfer analysis, 10 mM [$\text{U}-^{13}\text{C}$]fructose was dissolved in glucose-free DMEM and 10% dialysed FBS with 1% penicillin–streptomycin. The media were used to culture hepatocytes, ultimately yielding hepatocyte-conditioned media. For evaluating cell number, all cells were trypsinized and stained with trypan blue. For isotope-tracer experiments with [$\text{U}-^{13}\text{C}$]glucose or [$\text{U}-^{13}\text{C}$]fructose, labels were administered in glucose-free DMEM with 10% FBS and 1% penicillin–streptomycin in 100 mm cell-culture plates for 4 h (unless otherwise specified) and then cells were collected for LC–MS analysis. Except where indicated, 5 mM of each label was

administered. For LPC 18:1-D7 (Avanti Polar) labelling, 300,000 CaSki cells were plated in a 10 cm plate and allowed to attach to the plate overnight. Next, 20 µM LPC 18:1-D7 was dissolved in high-glucose DMEM containing 10% dialysed FBS and 1% penicillin–streptomycin. These media were then administered to the CaSki cells. The media were refreshed every 24 h. After 3 days, the cells were then collected for LC–MS analysis. Before collecting for LC–MS analysis, cells were washed once with PBS and then water. Cells were quenched with 1 ml of methanol per 100 mm plate (TPP), and cells were collected into a microcentrifuge tube by scraping. Methanol was removed from cells by using a nitrogen evaporator. The samples were then lyophilized for 12 h. The dried samples were weighed and extracted by using the metabolite extraction protocol below. PF-06835919 was administered to cells in DMSO at a final concentration of 30 µM or 250 µM in the culture media. These cell culture PF-06835919 experiments were done in DMEM containing 10 mM glucose and 10 mM fructose with 10% FBS and 1% penicillin–streptomycin. NBDG (Caymen) and NBDF (Caymen) uptake studies were performed based on previous work⁵⁸. In brief, the media were aspirated from cells that were plated in a 96-well plate at a uniform density. The cells were then incubated in PBS for 30 min and subsequently incubated in glucose-free DMEM and 10% dialysed FBS with 100 µM NBDG or NBDF for 30 min. After media removal and PBS rinsing, fluorescence was read on a Cyvation 5 microplate reader (Bitek) with an excitation of 475 nm and an emission of 550 nm while the cells were in PBS.

Primary mouse hepatocytes were isolated as described previously⁵⁹. The hepatocytes were plated on a collagen-coated Transwell (Corning). When co-cultured with CaSki cells, 1 × 10⁵ CaSki cells were plated on the upper insert of the Transwell containing hepatocytes. In the control conditions, 1 × 10⁵ CaSki cells were plated on both the insert and the bottom well. CaSki cells were collected from the upper inserts of both conditions for LC–MS analysis or determination of relative cell number by trypan blue staining.

Assessment of proliferating and quiescent (contact-inhibited) 3T3-L1 fibroblasts was performed as described previously⁴⁵. 3T3-L1 cells proliferate at lower cell densities and become quiescent at higher cell densities (Extended Data Fig. 7e). As described previously, 3T3-L1 cells were seeded at a plating density of 1.0 × 10⁴ cells per cm². To obtain proliferating cells, cells were collected for western blot analysis 30 h later. To obtain quiescent cells, cells were collected 150 h later.

To perform ex vivo culture of CaSki tumours, CaSki cells were first implanted into nude mice and allowed to grow for 21 days on a control diet + 10% fructose water. The resulting tumours were then removed, formed into a single-cell suspension, and plated ex vivo in DMEM media containing 5 mM glucose + 5 mM fructose for 5 h before the media were changed and cells were labelled with either 5 mM [$U-^{13}C$]glucose + 5 mM fructose ($n = 3$) or 5 mM [$U-^{13}C$]fructose + 5 mM glucose ($n = 3$) for 4 h. All media conditions contained 10% FBS and 1% penicillin–streptomycin.

Ex vivo culture of *BRAF/p53* zebrafish melanoma was performed by amputation of a melanoma from a euthanized fish, based on a previously applied protocol⁶⁰. A single-cell suspension of the isolated tumour was formed through incubation of the tumour at room temperature in a 0.075 mg ml⁻¹ solution of liberase (Millipore-Sigma) for 30 min. Disintegration of the tumour was encouraged by periodic pipetting. The suspension was filtered through a 40 µm filter (MidSci) to remove any aggregates of tumour and then centrifuged at 1,000 rpm for 5 min. The pellet was resuspended in DMEM containing 10% FBS, 1% penicillin–streptomycin, 1% GlutaMAX and no pyruvate before being transferred to fibronectin-coated plates (Corning) and cultured at 28.5 °C and 5% CO₂.

qPCR analysis

Total RNA was extracted from CaSki cells with Trizol according to the manufacturer's instructions. RNA was reversed transcribed to cDNA

by using the SuperScript III First-Strand Synthesis SuperMix. qPCR was performed by using the PowerUp SYBR Green Master Mix with a StepOnePlus RealTime PCR system (Applied Biosystems). *Gapdh* was used as a reference gene. Data were analysed using by the comparative C_t method.

Conjugation of LPC 18:1 to BSA

A 22.7 mg ml⁻¹ solution (100 ml) of ultra fatty-acid-free BSA (Millipore-Sigma) in glucose-free, glutamine-free DMEM (Life Technologies) was formed by heating with stirring for 1 h at 37 °C. A 50 ml aliquot of this solution was removed and 40 ml of glucose-free, glutamine-free DMEM (Life Technologies) was added to yield the BSA vehicle control. A 1.3 mg ml⁻¹ solution (44 ml) of LPC18:1 (Avanti Polar Lipids) was made with glucose-free, glutamine-free DMEM (Life Technologies). A 40 ml aliquot of this solution was added to 50 ml of the 22.7 mg ml⁻¹ BSA solution and stirred for 1 h at 37 °C.

Polar metabolite extraction

For mouse serum and cell-culture media extractions, 90 µl of 2:2:1 methanol:acetonitrile:water (M:A:W) was added to 10 µl of sample. For zebrafish serum extraction, 36 µl of M:A:W was added to 4 µl of sample. The samples were vortexed and placed at -20 °C for 1 h. The samples then were centrifuged at 4 °C for 10 min. The supernatant was removed and analysed by LC–MS. For tissue, frozen samples were first ground into a fine powder with a mortar and pestle in the presence of liquid nitrogen. The powder was weighed and 1 ml M:A:W was added per 5 mg of tissue weight. For tumours, the entire sample was extracted. For cell-culture samples, 1 ml of M:A:W was added per 1 mg of lyophilized cell pellet. Tissue and cell-culture samples were then vortexed for 30 s, placed in liquid nitrogen for 1 min and sonicated for 10 min. This cycle was repeated three times. The samples were subsequently maintained at -20 °C for 1 h, centrifuged at 14,000 rpm for 10 min and the supernatants were then transferred to new microcentrifuge tubes. The M:A:W solvent was evaporated under nitrogen, and the samples were resuspended in 60:40 acetonitrile:water with a normalization of 40 µl per mg of initial lyophilized cell pellet or tissue weight. The above extraction methods were used for all targeted analysis of LPCs PCs, and fatty acids.

Extraction of non-polars for untargeted profiling

Non-polar metabolite extractions were performed as described previously⁶¹. For extractions of mouse serum and cell-culture medium, 50 µl of biofluid was added to a Captiva EMR 96 well plate (Agilent). Acetonitrile:methanol (1:1, 200 µl) with labelled internal standards was added to the plate and incubated for 1 min on a plate shaker and at 4 °C for 10 min. M:A:W (2:2:1, 150 µl) was added to the plate and eluted by using a positive pressure manifold into a collection plate. The Captiva EMR 96-well plate was washed one additional time with M:A:W (2:2:1). For non-polar metabolites, a new collection plate was used and eluted with 1:1 methanol:methyl tert-butyl ether. Eluted non-polar metabolites were dried under a stream of N₂ by a Biotage N₂-dryer. Non-polar metabolites were reconstituted in 1:1 isopropanol:methanol.

Western blots

Cells or tissues were harvested in RIPA buffer (Thermo Fisher Scientific) with a protease inhibitor cocktail (Thermo Fisher Scientific). Each sample was sonicated for 30 s, and the resulting lysates were separated on SDS–PAGE under reducing conditions. Protein bands were transferred to a PVDF membrane. Immunoblotting was performed with anti-ketohexokinase (Santa Cruz), anti-ketohexokinase-C (Signalway), anti-ketohexokinase-A (Signalway), anti-sorbitol dehydrogenase (Santa Cruz), anti-alcohol dehydrogenase (Santa Cruz) or anti-LPCAT1 (Proteintech). Anti-β-tubulin (Cell Signaling), anti-β-actin (Cell Signaling) or anti-succinate dehydrogenase (Cell Signaling) was used as

Article

a loading control. Anti-rabbit and anti-mouse secondary antibodies were from Cell Signaling. Blots were imaged on a LI-COR C Digit blot scanner (LI-COR). Mouse hepatocytes and primary human hepatocytes (Millipore-Sigma) for western blot analyses were collected as described above. Uncropped, full size blots are shown in Supplementary Fig. 1.

Silencing of sorbitol dehydrogenase and LPCAT1

Sorbitol dehydrogenase and LPCAT1 were silenced by using a collection of siRNA duplexes targeting human *SORD* (TriFECTa, IDT; hs.Ri.SORD.13) or *LPCAT1* (TriFECTa, IDT; hs.Ri.LPCAT1.13.1). Lipofectamine RNAiMAX transfection reagent (Invitrogen) was used for the transfection according to the manufacturer's instructions. Scrambled siRNA (TriFECTa, IDT) was used as a negative control. The knockdown efficiency was assessed via western blotting. Cell number was assessed after 4 days of *SORD* siRNA administration and 3 days after *LPCAT1* siRNA administration.

LC-MS analysis

LC-MS analysis of polar metabolites was performed by using a SeQuant ZIC-pHILIC column (EMD Millipore) interfaced with an Agilent 6540 Q-TOF. Unless otherwise indicated, a 150×2.1 mm, $5\text{ }\mu\text{m}$ SeQuant ZIC-pHILIC column was used with an Agilent 1290 Infinity II LC system, applying methods established previously⁶². Mobile-phase solvents had the following composition: (A) 20 mM ammonium acetate in water:acetonitrile (95:5) and (B) 100% acetonitrile. The following linear gradient was used: 0–0.5 min, 90% B; 0.5–30 min, 90–30% B; 30–31 min, 30% B. Injection volumes were 2 μl for all experiments. The column compartment was maintained at 45 °C. The mass range was set to 50 to 1,500 m/z . Instrument parameters were as follows: gas, 200 °C at 4 l min^{-1} ; nebulizer, 44 psi at 2,000 V; sheath gas, 300 °C at 12 l min^{-1} ; capillary, 3,000 V; fragmentor, 100 V; skimmer, 65 V; and scan rate, 3 scans per second. The instrument was operated in negative ionization mode for all of the samples analysed.

LC-MS of non-polar metabolites was performed as reported previously⁶¹. In brief, the samples were analysed by using an HSS T3 column (Acquity; 150×2.1 mm, $1.8\text{ }\mu\text{m}$) interfaced with an Agilent 6545 Q-TOF. The LC system used was an Agilent 1290 Infinity II. Mobile-phase solvents had the following composition: (A) 60% acetonitrile, 40% water, 0.1% formic acid, 10 mM ammonium formate 2.5 μM medronic acid and (B) 90% 2-propanol, 10% acetonitrile, 0.1% formic acid, 10 mM ammonium formate. The following linear gradient was used: 0–2 min, 30% B; 17 min, 75% B; 20 min, 85% B; 23–26 min, 100% B; 26 min, 30% B. Injection volumes were 4 μl . The column compartment was maintained at 60 °C. The mass range was 120–1,200 m/z . Instrument parameters were as follows: gas, 250 °C at 11 l min^{-1} ; nebulizer pressure, 35 psi; sheath gas temperature, 300 °C; sheath gas flow, 12 l min^{-1} ; VCap, 3,000 V; nozzle voltage, 500 V; Fragmentor, 160 V; Skimmer, 65 V. The instrument was operated in positive ionization mode for all samples analysed.

To separate fructose 1-phosphate from other hexose phosphates, a $2\text{ mm} \times 150$ mm HILICpak VT-50-2D column (Shodex) was used with an isocratic flow of 80% acetonitrile, 20% water and 25 mM ammonium formate. The flow rate was 0.150 ml min^{-1} . All other experimental conditions were kept as above.

Metabolites were quantified by using ^{13}C -labelled or ^2H -labelled internal standards or a standard curve. Metabolite identifications represent level 1 or level 2 confidence according to the Metabolomics Standards Initiative⁶³. All LPC and hexose phosphate identifications were confirmed with authentic standards and are level 1 confidence. In the LC-MS methods we used here, LPC 18:1/0:0 and LPC 0:0/18:1 as well as LPC 18:2/0:0 and LPC 0:0/18:2 have different retention times. Throughout this study, when we report LPC 18:1 or LPC 18:2, we only considered the signals corresponding to LPC18:1/0:0 and LPC18:2/0:0, respectively.

LC-MS data analysis

Data processing was accomplished by using XCMS⁶⁴. Lipid species were annotated by uploading MS/MS spectra of pooled samples into Agilent MassHunter Lipid Annotator (v.1.0)⁶⁵. Peaks were extracted by using Skyline (v.21.2)⁶⁶.

For untargeted metabolomics, centred peaks were uploaded to MetaboAnalyst (v.5.0)⁶⁷ and were normalized (mean centred and divided by the s.d. of each variable). Heat maps were generated from normalized data. Metabolites or lipids were compared by using one-way ANOVA (FDR $P < 0.05$). For over-representation analysis metabolite set enrichment analyses, significantly increased lipids in HFCS versus control conditions (according to a *t* test) were analysed by using MetaboAnalyst v.5.0. A reference metabolite set library was selected (SMPDB/Kegg for metabolites or main class for lipids). An enrichment ratio was computed by dividing the number of hits by the expected number of hits for a metabolite set. Unless otherwise stated, FDR < 0.05 was considered to be statistically significant. Isotopologues were generated within Skyline or within MassHunter (Agilent). Fractional carbon atom enrichment was determined as reported previously⁶⁸.

Isotopologue plots

Isotopologues are molecules that differ only in their isotopic composition. For example, a given metabolite with one ^{13}C label is a different isotopologue than that same metabolite with two ^{13}C labels. When an isotope tracer is processed through different metabolic pathways, it produces different isotopologues^{69,70}. For instance, when U- ^{13}C glucose is metabolized by the pyruvate dehydrogenase complex and citrate synthase uses a non-labelled oxaloacetate, it produces M+2 citrate⁷¹. By contrast, when U- ^{13}C -glucose is metabolized by pyruvate carboxylase and citrate synthase uses a non-labelled acetyl-CoA, it produces M+3 citrate. An isotopologue distribution plot shows the proportion or percentage of each isotopologue for the metabolite of interest. M+0 represents the unlabelled metabolite with no ^{13}C labels. M+1, M+2 and M+3 represent a metabolite with one ^{13}C label, two ^{13}C labels and three ^{13}C labels, respectively. Isotopologue plots span from M+0 to M+n, where n is the total number of carbons in the metabolite of interest. The sum of all isotopologues should be 100%. We include statistical comparisons between each pair of isotopologues. Plots of isotopologue distributions are not natural-abundance corrected, unless otherwise noted. Data for total ^{13}C labelling (for example, the sum of all isotopologues for a given lipid species) were corrected for natural abundance.

Analysis of data from patients with cervical cancer

Patients with cervical cancer included in this study ($n = 99$) were enrolled in a prospective tumour banking study with written informed consent (201105374), and data were analysed with institutional review board approval with waiver of consent. All of the patients in this cohort were uniformly treated with curative-intent chemoradiation and clinical data were prospectively collected, including outcome data and FIGO stage. Primary cervical cancer samples with sufficient high-quality RNA, as defined by the criteria utilized for TCGA⁷², were included in this study for whole-transcriptome sequencing (RNA-seq; Gene Expression Omnibus: GSE275914). Poly(A) selection and multiplexed sequencing (Illumina HiSeq 2500, 1 \times 50 nucleotides, ~40 million reads per sample) were performed at the Genome Technology Access Center (GTAC) at Washington University School of Medicine. RNA-seq reads were aligned to the Genome Reference Consortium Human Build 38 (GRCh38) by using STAR2 with Ensembl genes for *Homo sapiens* version 90. Isoform expression levels for *KHK-A* and *KHK-C* were calculated and normalized as fragments per kilobase per million reads by using Cufflinks with the default parameters^{73,74}. Integrative genomics viewer (IGV) was used to visualize and manually

inspect sequencing reads from isoform specific exons⁵⁶. The Kaplan–Meier estimator was used to estimate recurrent-free survival and overall survival based on *KHK-A* expression levels, and significance levels from a log-rank test are reported.

Statistics

Statistical analyses were performed by using GraphPad Prism (v.9.2) for Windows (GraphPad). Data are reported as mean \pm s.d. or mean \pm s.e.m. where indicated. For all comparisons with two conditions, an unpaired, two-tailed *t*-test was used. For all comparisons with three or more conditions, unless otherwise indicated, one-way ANOVA or two-way ANOVA was used followed by Dunnett's or Tukey's post hoc test. Data were log transformed when assumptions of normality were not met, and a Mann–Whitney *U*-test or a Kruskal–Wallis test with Dunn's post hoc test was used. Comparisons of incidence were performed by using two-tailed Fisher's exact tests. Unless otherwise stated, $P < 0.05$ was considered to be statistically significant. Sample sizes were based on previous experimental experience in our research group and previous studies in the literature.

Reporting summary

Further information on research design is available in the Nature Portfolio Reporting Summary linked to this article.

Data availability

RNA-seq data were deposited at the Gene Expression Omnibus under accession number GSE275914. Source data are provided with this paper. LC–MS data were uploaded to the Metabolomics Workbench under project identifier PR002203.

48. Sullivan, M. R. et al. Quantification of microenvironmental metabolites in murine cancers reveals determinants of tumor nutrient availability. *eLife* **8**, e44235 (2019).
49. Kaufman, C. K. et al. A zebrafish melanoma model reveals emergence of neural crest identity during melanoma initiation. *Science* **351**, aad2197 (2016).
50. Naser, F. J. et al. Isotope tracing in adult zebrafish reveals alanine cycling between melanoma and liver. *Cell Metab.* **33**, 1493–1504 (2021).
51. Kent, W. J. et al. The human genome browser at UCSC. *Genome Res.* **12**, 996–1006 (2002).
52. Madeira, F. et al. The EMBL-EBI search and sequence analysis tools APIs in 2019. *Nucleic Acids Res.* **47**, W636–W641 (2019).
53. Leinonen, R., Sugawara, H. & Shumway, M. The sequence read archive. *Nucleic Acids Res.* **39**, D19–D21 (2011).
54. Dobin, A. et al. STAR: ultrafast universal RNA-seq aligner. *Bioinformatics* **29**, 15–21 (2013).
55. Trapnell, C. et al. Differential gene and transcript expression analysis of RNA-seq experiments with TopHat and Cufflinks. *Nat. Protoc.* **7**, 562–578 (2012).
56. Robinson, J. T. et al. Integrative genomics viewer. *Nat. Biotechnol.* **29**, 24–26 (2011).
57. Souroullas, G. P. et al. An oncogenic Ezh2 mutation induces tumors through global redistribution of histone 3 lysine 27 trimethylation. *Nat. Med.* **22**, 632–640 (2016).
58. Levi, J. et al. Fluorescent fructose derivatives for imaging breast cancer cells. *Bioconjug. Chem.* **18**, 628–634 (2007).
59. McCommis, K. S. et al. Loss of mitochondrial pyruvate carrier 2 in liver leads to defects in gluconeogenesis and compensation via pyruvate-alanine cycling. *Cell Metab.* **22**, 682–694 (2015).
60. Heilmann, S. et al. A quantitative system for studying metastasis using transparent zebrafish. *Cancer Res.* **75**, 4272–4282 (2015).
61. Sindelar, M. et al. Longitudinal metabolomics of human plasma reveals prognostic markers of COVID-19 disease severity. *Cell Rep. Med.* **2**, 100369 (2021).
62. Spalding, J. L., Naser, F. J., Mahieu, N. G., Johnson, S. L. & Patti, G. J. Trace phosphate improves ZIC-pHILIC peak shape, sensitivity, and coverage for untargeted metabolomics. *J. Proteome Res.* **17**, 3537–3546 (2018).
63. Summer, L. W. et al. Proposed minimum reporting standards for chemical analysis: Chemical Analysis Working Group (CAWG) Metabolomics Standards Initiative (MSI). *Metabolomics* **3**, 211 (2007).
64. Mahieu, N. G., Genenbacher, J. L. & Patti, G. J. A roadmap for the XCMS family of software solutions in metabolomics. *Curr. Opin. Chem. Biol.* **30**, 87–93 (2016).
65. Koelmel, J. P. et al. Lipid annotator: towards accurate annotation in non-targeted liquid chromatography high-resolution tandem mass spectrometry (LC–HRMS/MS) lipidomics using a rapid and user-friendly software. *Metabolites* **10**, 101 (2020).
66. Adams, K. J. et al. Skyline for small molecules: a unifying software package for quantitative metabolomics. *J. Proteome Res.* **19**, 1447–1458 (2020).
67. Pang, Z. et al. MetaboAnalyst 5.0: narrowing the gap between raw spectra and functional insights. *Nucleic Acids Res.* **49**, W388–W396 (2021).
68. Schwaiger-Haber, M. et al. Using mass spectrometry imaging to map fluxes quantitatively in the tumor ecosystem. *Nat. Commun.* **14**, 2876 (2023).
69. Buescher, J. M. et al. A roadmap for interpreting ¹³C metabolite labeling patterns from cells. *Curr. Opin. Biotechnol.* **34**, 189–201 (2015).
70. Llufrío, E. M., Cho, K. & Patti, G. J. Systems-level analysis of isotopic labeling in untargeted metabolomic data by X13CMS. *Nat. Protoc.* **14**, 1970–1990 (2019).
71. Chen, P. H. et al. Metabolic diversity in human non-small cell lung cancer cells. *Mol. Cell* **76**, 838–851 (2019).
72. Burk, R. D. et al. Integrated genomic and molecular characterization of cervical cancer. *Nature* **543**, 378–384 (2017).
73. Liao, Y., Smyth, G. K. & Shi, W. FeatureCounts: an efficient general purpose program for assigning sequence reads to genomic features. *Bioinformatics* **30**, 923–930 (2014).
74. Trapnell, C. et al. Transcript assembly and quantification by RNA-Seq reveals unannotated transcripts and isoform switching during cell differentiation. *Nat. Biotechnol.* **28**, 511–515 (2010).

Acknowledgements We acknowledge funding from the National Institutes of Health grants P30DK056341 and R35 ES028365 (G.J.P.). R.F.-G. was supported by the TL1 Translational Sciences Postdoctoral Program (TL1TR002344). J.L.R. was supported by the Siteman Cancer Biology Pathway Program (T32CA113275 and P30CA091842). We thank S. L. Johnson (posthumous) for his scientific insights in the early stages of this work; R. W. Gross for his input on lipid biochemistry; and M. W. Stoner for her graphical assistance with figure creation.

Author contributions R.F.-G., J.L.R., I.S., Y.W., M.S.-H., A.J.D., M.Z., F.J.N., M.M.J., J.L.S., S.C., K.S.M., E.T.K. and S.M.Z. performed in vitro and in vivo ¹³C-labelling experiments, tissue collection for metabolomics experiments, in vitro cell growth assays, mouse and zebrafish tumour growth experiments, and LC–MS analysis. R.F.-G., K.J., M.I. and J.Z. performed analysis of genetic data from human patients and zebrafish. R.F.-G., R.E.D., G.P.S., B.N.F., L.P.S., C.K.K., J.K.S., J.Z. and G.J.P. designed experiments and led data interpretation. R.F.-G. and G.J.P. wrote the manuscript, with input from all of the authors. All of the authors contributed to revisions.

Competing interests B.N.F. is a stockholder and member of the scientific advisory board of Cirius Therapeutics. G.J.P. is a scientific advisory board member for Cambridge Isotope Laboratories and has a collaborative research agreement with Agilent Technologies. G.J.P. is the Chief Scientific Officer of Panome Bio.

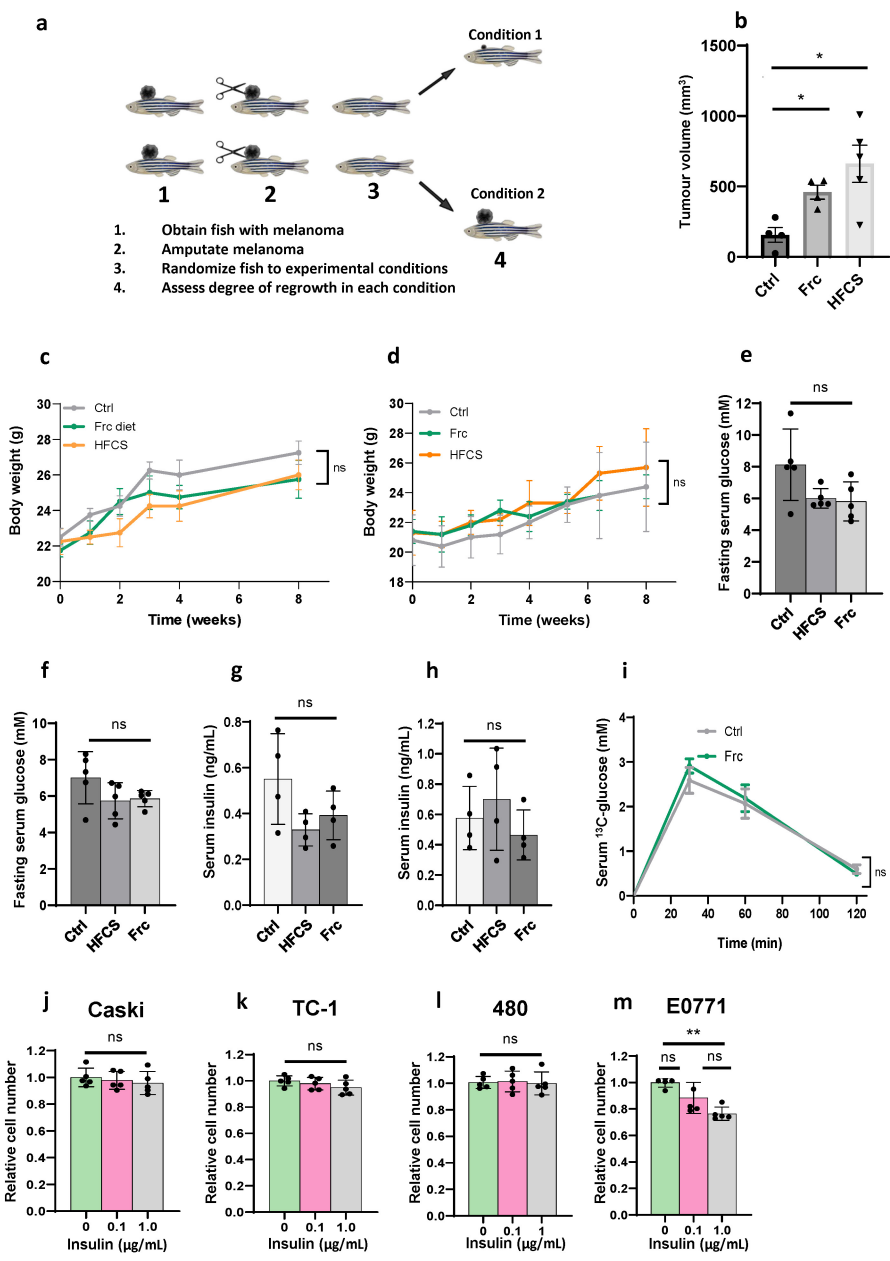
Additional information

Supplementary information The online version contains supplementary material available at <https://doi.org/10.1038/s41586-024-08258-3>.

Correspondence and requests for materials should be addressed to Gary J. Patti.

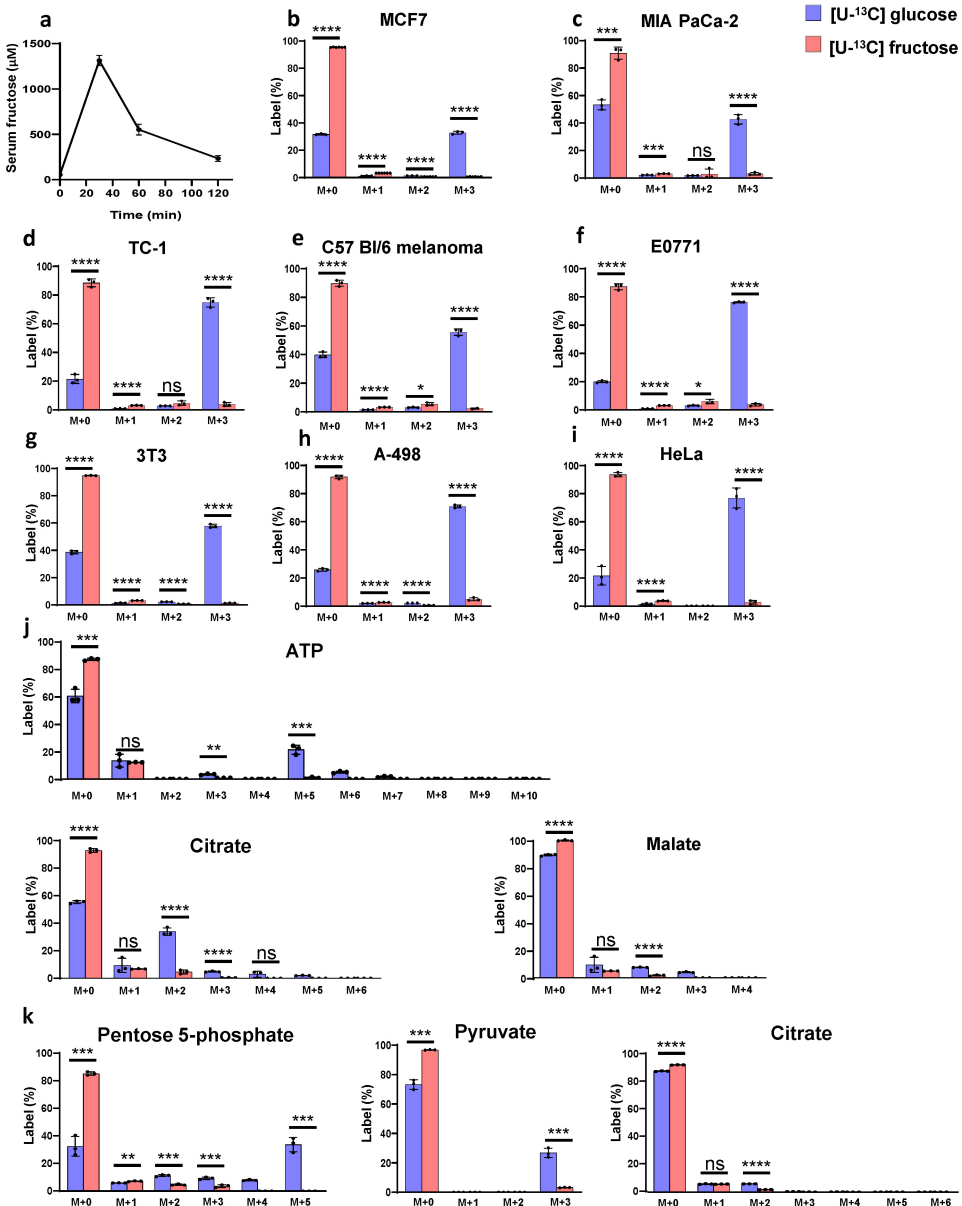
Peer review information *Nature* thanks Douglas Mashek and the other, anonymous, reviewers for their contribution to the peer review of this work.

Reprints and permissions information is available at <http://www.nature.com/reprints>.



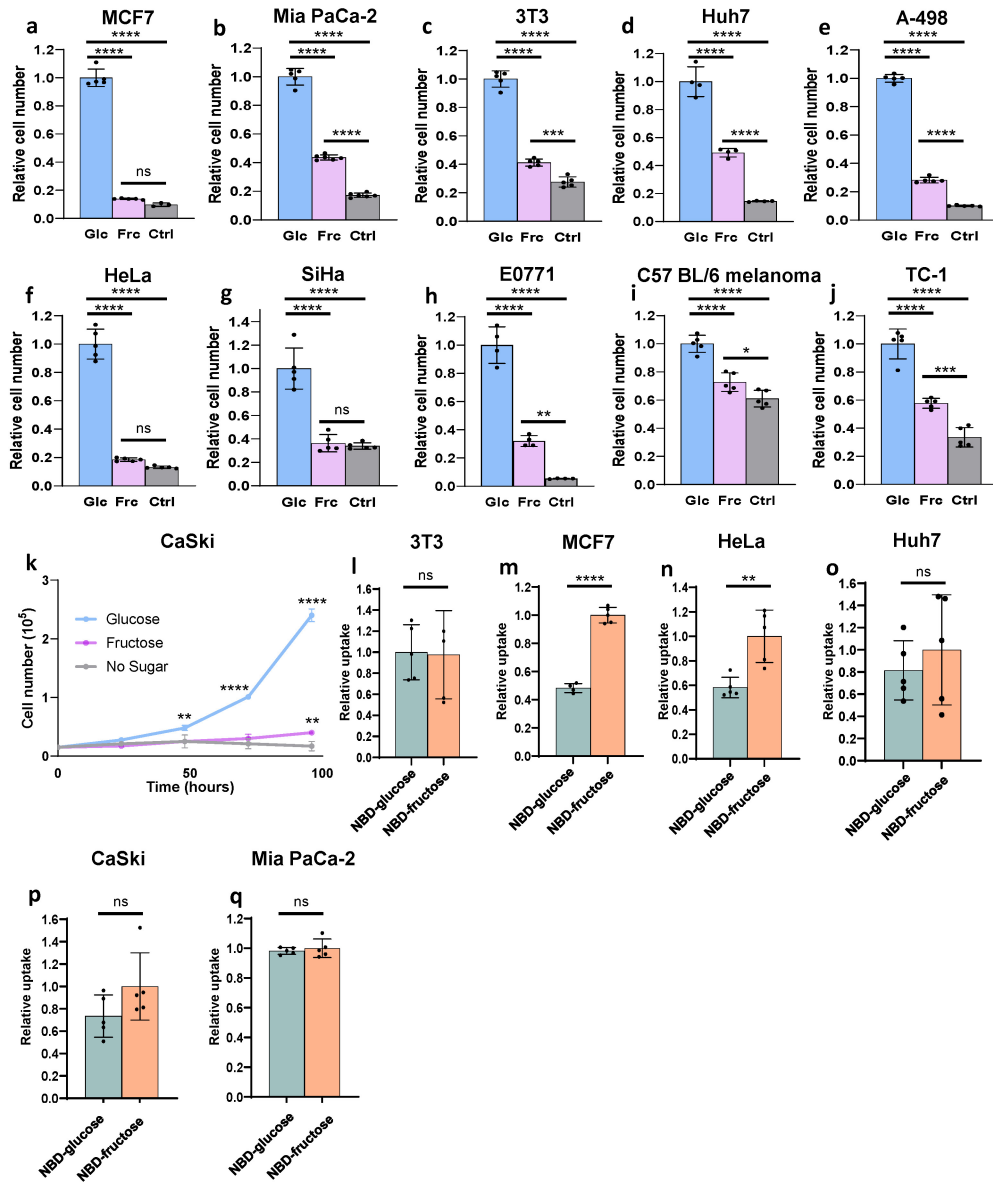
Extended Data Fig. 1 | Dietary fructose increases tumour growth without inducing metabolic syndrome in our models. (a) Schematic of zebrafish melanoma regrowth assay. Image created with Biorender.com. For (b-h), mice were administered a control diet (Ctrl), high-fructose diet (Frc diet), control diet + 10% fructose water (Frc), or control diet + 20% HFCS water (HFCS). Mice were administered the diets for 8 weeks (c,d) or 6 weeks (e-h). (b) Tumour volumes two weeks after HPV E6/E7-expressing TC-1 cells were orthotopically implanted into the cervix of C57 BL/6 mice (Ctrl, n = 4; Frc, n = 4; HFCS, n = 5). (c) Body weight of nude mice (n = 4 per condition). (d) Body weight of C57 BL/6 mice (Ctrl, n = 5; Frc, n = 5 and HFCS, n = 6). (e) Fasting serum glucose concentrations in nude mice (n = 5 per condition). (f) Fasting serum glucose concentrations in C57 BL/6 mice (n = 5 per condition). (g) Fasting serum insulin

concentrations in nude mice (n = 4 per condition). (h) Fasting serum insulin concentrations in C57 BL/6 mice (n = 4 per condition). (i) Alanine tolerance test performed on C57 BL/6 mice after administering a control diet (Ctrl, n = 4) or a control diet + 10% fructose water (Frc, n = 4) for six weeks. Mice were gavaged with 0.5 g/kg [$\text{U}-^{13}\text{C}$] alanine and serum ^{13}C -glucose production was assessed. (j)-(m) Relative cell number (n = 5) after 4 days of culture at the indicated concentrations of insulin in DMEM + 0.1% FBS. All experiments in this figure were performed once. P values determined by ordinary one-way ANOVA with Tukey's multiple comparisons test (b, e-h, j-m) or two-way ANOVA with Šídák's multiple comparisons test (c, d, i). *P < 0.05, **P < 0.01, ***P < 0.001, ****P < 0.0001, and n.s. is not significant. Data in (b) shown as mean \pm S.E.M. All remaining data shown as mean \pm standard deviation.

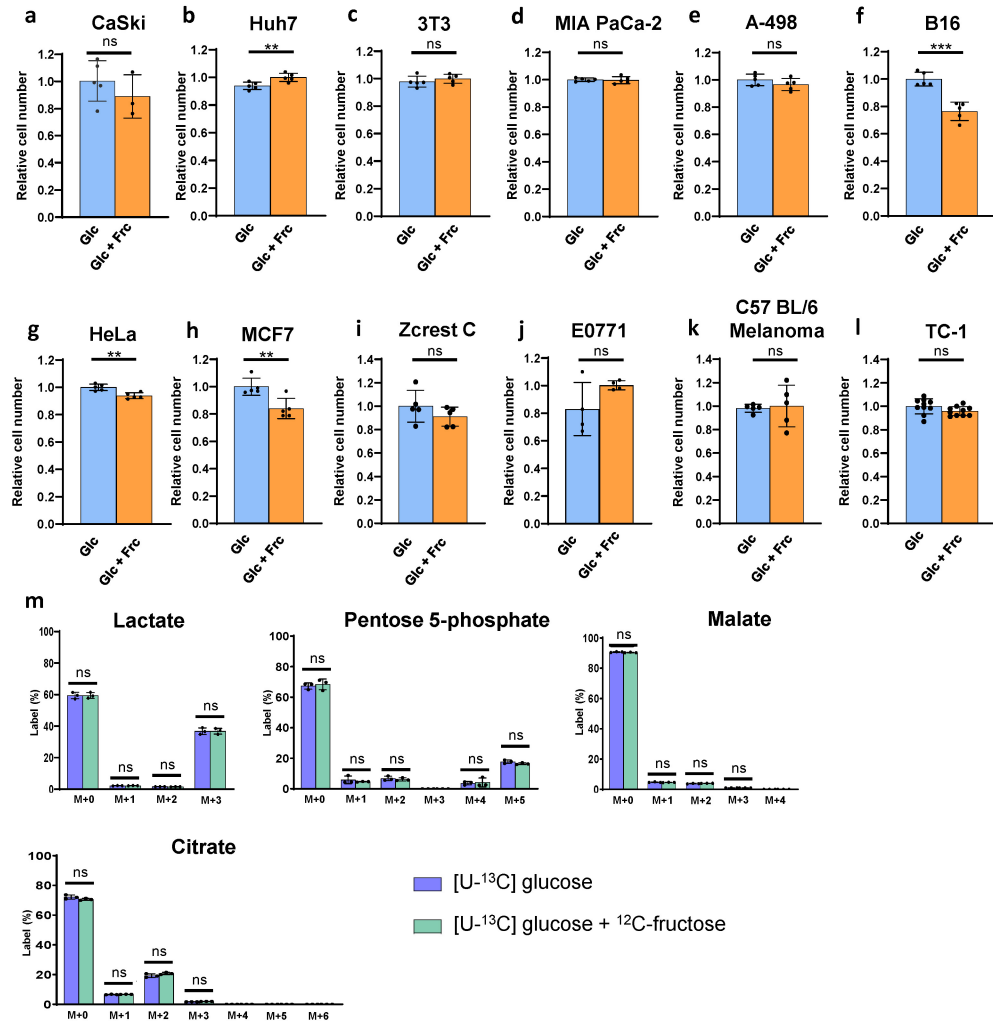


Extended Data Fig. 2 | Transformed cells do not efficiently metabolize fructose. (a) Serum fructose levels after intraperitoneal injection of 1 g/kg fructose to C57BL/6 mice ($n = 5$). (b-i) Isotopologue distribution for lactate after 4 h of labelling the indicated cell lines with either [U-¹³C] glucose ($n = 3$) or [U-¹³C] fructose ($n = 3-6$). (j) Isotopologue distributions for the indicated metabolites of central carbon metabolism after 4 h of labelling CaSkI cells with either [U-¹³C] glucose ($n = 3$) or [U-¹³C] fructose ($n = 3$). (k) Isotopologue

distributions for the indicated metabolites of central carbon metabolism after 4 h of labelling BRAF/p53 zebrafish melanoma with either [U-¹³C] glucose ($n = 3$) or [U-¹³C] fructose ($n = 3$). All experiments in this figure were performed once. * $P < 0.05$, ** $P < 0.01$, *** $P < 0.001$, **** $P < 0.0001$, and n.s. is not significant. P-values determined by multiple unpaired T-tests. All data shown as mean \pm standard deviation.

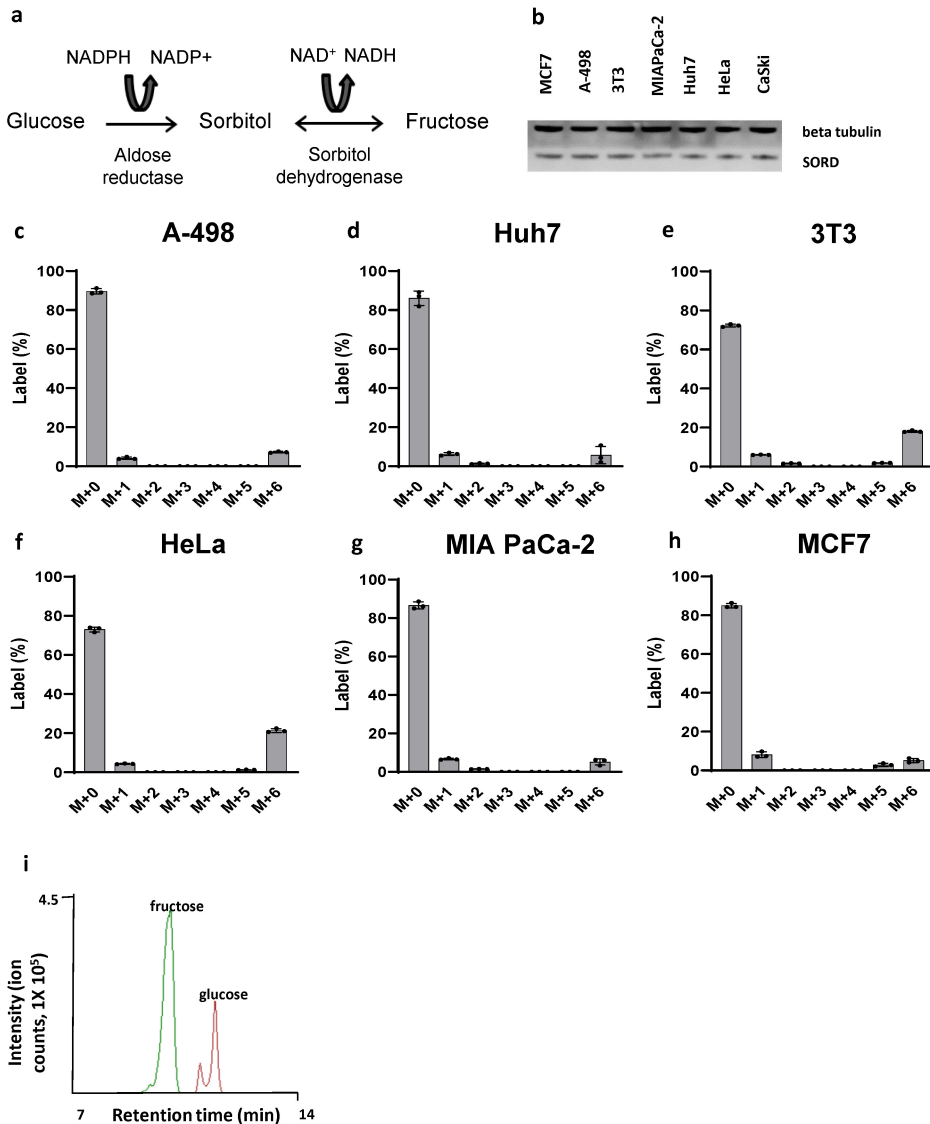


contain 10% FBS and 1% pen/strep. **(l-q)** Relative intracellular fluorescence signal following a 30-minute incubation with either 2-NBDG (n = 3-5) or 1-NBDF (n = 3-5). P values determined by ordinary one-way ANOVA with Tukey's multiple comparisons test (a-j), two-way ANOVA with Šídák's multiple comparisons test with all conditions compared to the control condition at each timepoint (k), or two-sided T-test (l-q). *P < 0.05, **P < 0.01, ***P < 0.001, ****P < 0.0001, and ns is not significant. All data shown as mean ± standard deviation.



Extended Data Fig. 4 | Addition of fructose to glucose-containing media does not enhance proliferation or alter metabolism. (a-l) Relative cell number after culturing the indicated cell lines in DMEM containing 20 mM glucose (Glc, n = 4-10) or 10 mM glucose + 10 mM fructose (Glc + Frc, n = 3-10) for 4 days. Media also contained 10% FBS and 1% pen/strep. (m) Isotopologue distributions for the indicated central carbon metabolites from CaSki cells that were

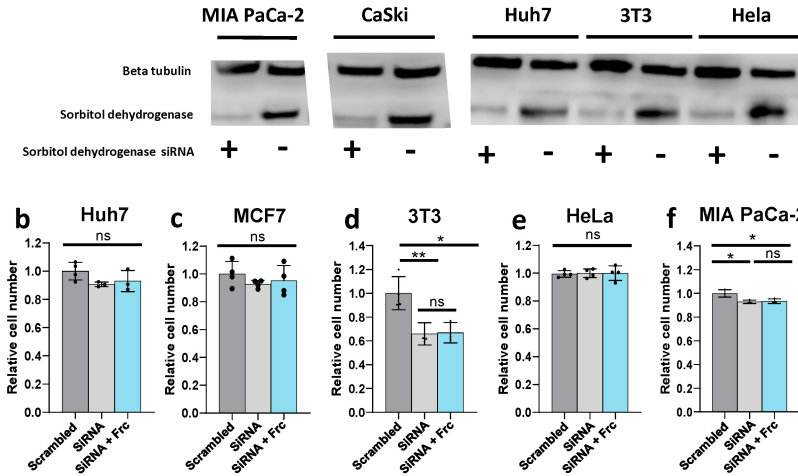
cultured with either 10 mM [$U\text{-}^{13}\text{C}$] glucose (n = 3) or 10 mM [$U\text{-}^{13}\text{C}$] glucose + 10 mM ^{12}C -fructose (n = 3) for 4 h. ^{12}C -fructose indicates unlabeled fructose. All experiments in this figure were performed once. P-values determined by two-sided T-test (a-l) and multiple unpaired T-tests (m). *P < 0.05, **P < 0.01, ***P < 0.001, ****P < 0.0001, and n.s. is not significant. All data shown as mean \pm standard deviation.



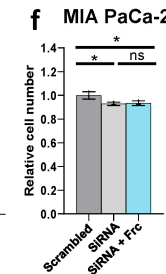
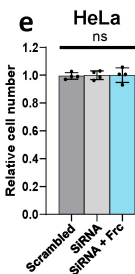
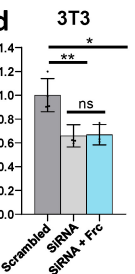
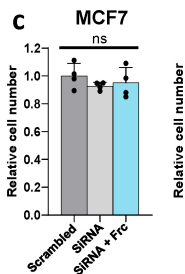
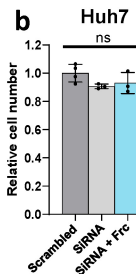
Extended Data Fig. 5 | Transformed cells produce endogenous fructose from glucose via fructoneogenesis. (a) Schematic depicting the polyol pathway and the generation of endogenous fructose from glucose. (b) Western blot analysis of sorbitol dehydrogenase from the indicated cell lines. (c-h) Isotopologue distribution for intracellular fructose after labelling the indicated cell lines

with 5 mM [$U^{13}\text{C}$] glucose for 4 h ($n = 3$). (i) Fructose and glucose are chromatographically resolved with a pHILIC column (see Methods). Data in b are representative of two independent experiments. All other experiments were performed once. All data shown as mean \pm standard deviation.

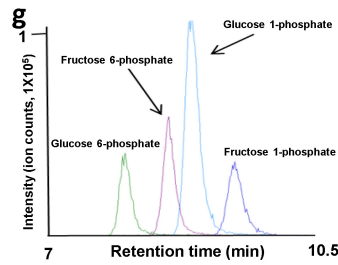
a



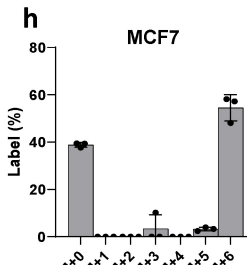
b



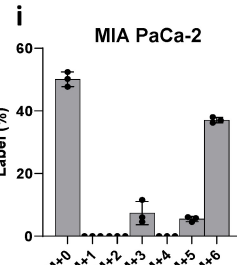
g



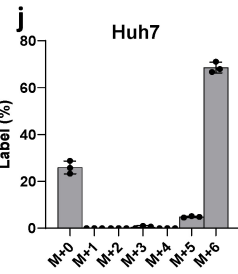
h



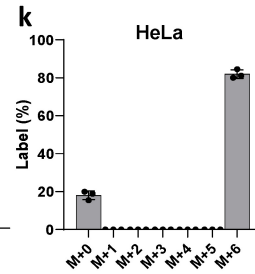
i



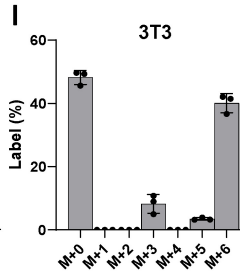
j



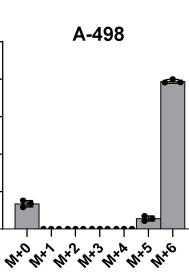
k



l



m

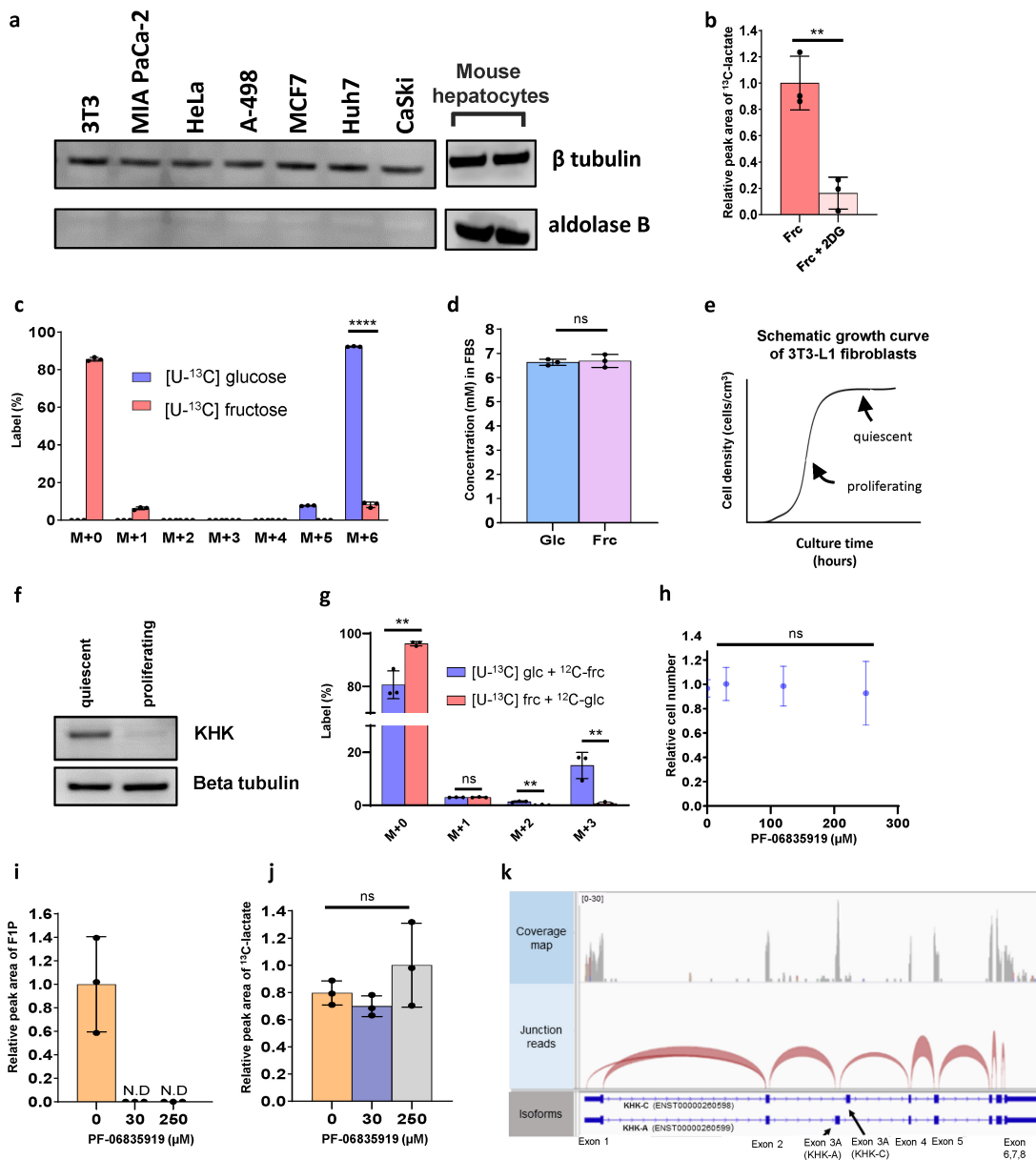


Extended Data Fig. 6 | Endogenous fructose has no impact on cell proliferation.

proliferation. (a) Western blot analysis of sorbitol dehydrogenase from the indicated cell lines after transfection with either sorbitol dehydrogenase siRNA (+) or scrambled control (-). (b-f) Relative cell number after administering sorbitol dehydrogenase siRNA (SORD siRNA, n = 3-4), scrambled control siRNA (scrambled control, n = 3-5), or sorbitol dehydrogenase siRNA and 10 mM fructose (SORD siRNA + 10 mM fructose, n = 3-4) to the indicated cell lines for 4 days. (g) Analysis of 15 μ M solutions of glucose 6-phosphate, fructose 6-phosphate, glucose 1-phosphate, and fructose 1-phosphate with a HILICpak

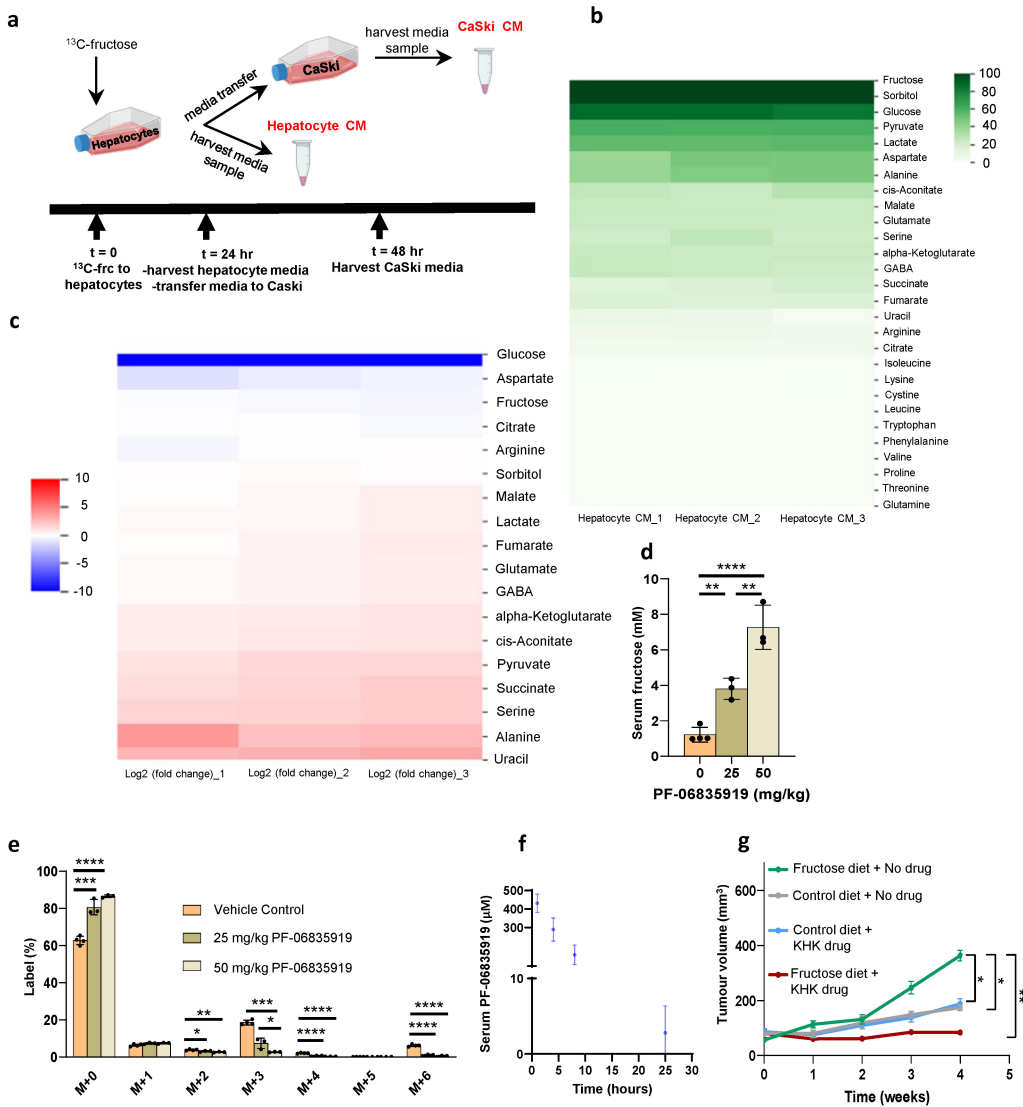
VT 50-2D column. Each is chromatographically resolved from one another. Solutions were prepared by using authentic standards. (h-m) Isotopologue distribution for fructose 1-phosphate after labelling with [$U^{13}\text{C}$] fructose for 4 h (n = 3). Labelled fructose 1-phosphate indicates KHK activity. All experiments in this figure were performed once. (b-f) P values determined by ordinary one-way ANOVA with Tukey's multiple comparisons test. *P < 0.05, **P < 0.01, ***P < 0.001, ****P < 0.0001, and n.s. is not significant. All data shown as mean \pm standard deviation.

Article



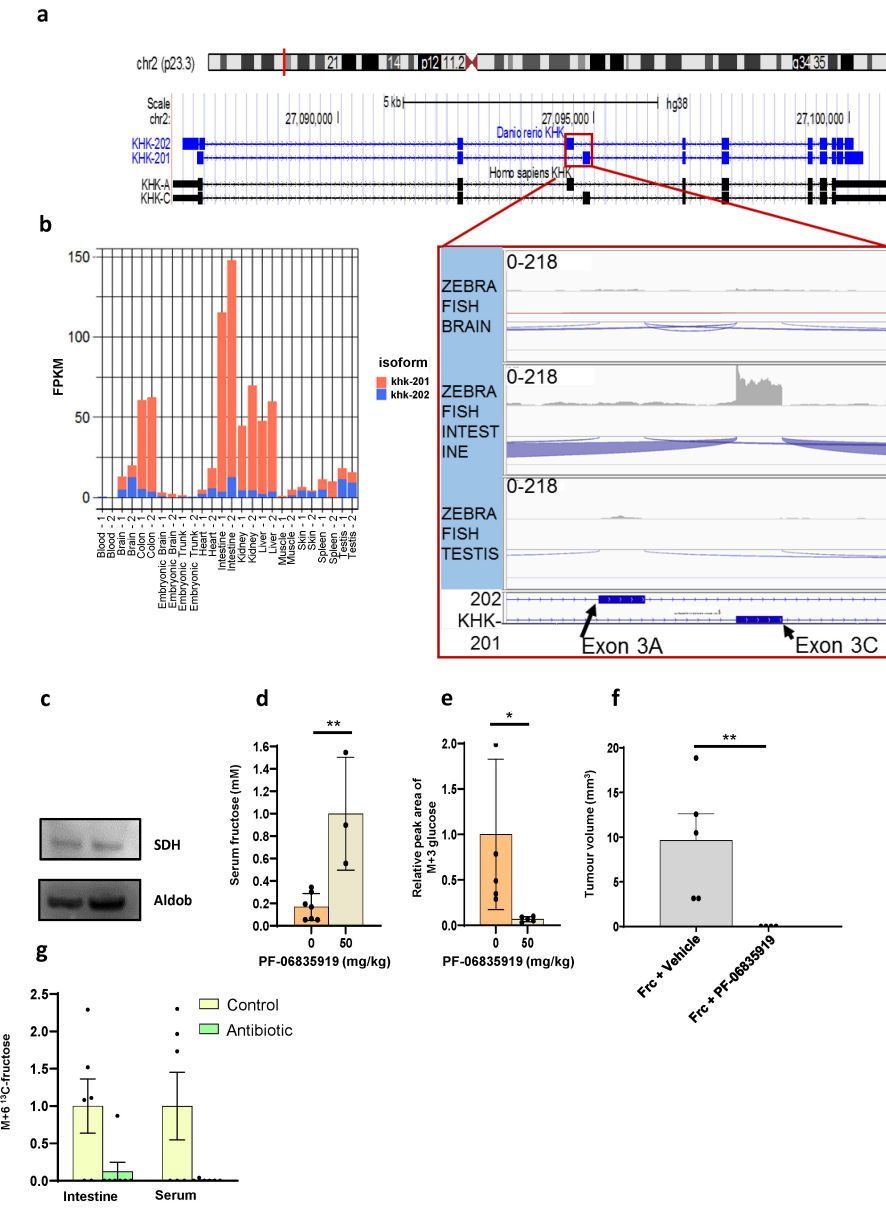
Extended Data Fig. 7 | KHK-C and aldolase B are absent in tested cancer cell lines. (a) Western blot analysis of aldolase B from the indicated cell lines or mouse hepatocytes. (b) Total ^{13}C -labelled lactate from CaSki cells treated with 5 mM [^{13}C] fructose (Frc, n = 3) or 5 mM [^{13}C] fructose + 20 mM 2DG (Frc + 2DG, n = 3). (c) Isotopologue distribution for fructose 6-phosphate after labelling CaSki cells with [^{13}C] fructose (n = 3) or [^{13}C] glucose (n = 3) for 4 h. (d) Concentration of glucose (Glc, n = 3) and fructose (Frc, n = 3) in fetal bovine serum. (e) Schematic of proliferating 3T3-L1 fibroblasts becoming quiescent at high cell densities when contact inhibited. (f) Western blot analysis of KHK from quiescent and proliferating 3T3-L1 fibroblasts. (g) Isotopologue distribution for lactate from CaSki tumours plated ex vivo. CaSki tumours were harvested from mice supplemented with 10% fructose water for 21 days. Single-cell suspensions were formed and plated ex vivo in media containing 5 mM [^{13}C] glucose + 5 mM ^{12}C -fructose (n = 3) or 5 mM [^{13}C] fructose + 5 mM ^{12}C -glucose (n = 3) for 4 h. ^{12}C -fructose (^{12}C -frc) and ^{12}C -glucose (^{12}C -glc)

indicate unlabeled fructose and glucose, respectively. (h) CaSki cell number as a function of PF-06835919 concentration (n = 3 per dose). Cells were cultured with 10 mM glucose and 10 mM fructose. (i) Total fructose 1-phosphate from CaSki cells after treatment with vehicle (n = 3), 30 μM (n = 3), or 250 μM PF-06835919 (n = 3). Cells were cultured with 10 mM glucose and 10 mM fructose. N.D. represents “not detected”. (j) Total ^{13}C -labelled lactate from CaSki cells treated with 5 mM [^{13}C] fructose together with either vehicle control (Ctrl, n = 3), 30 μM (n = 3), or 250 μM of PF-06835919 (n = 3). (k) An Integrative Genomics Viewer (IGV) view of KHK gene expression from a cervical tumour shows expression of only Exon 3 A that is specific to KHK-A. Data in a and d are representative of two independent experiments. All other experiments were performed once. P values determined by a two-sided T-test (b, c, d), an unpaired T-test (g), or ordinary one-way ANOVA with Tukey’s multiple comparisons test (h, j). *P < 0.05, **P < 0.01, ***P < 0.001, ****P < 0.0001, and n.s. is not significant. All data shown as mean \pm standard deviation.



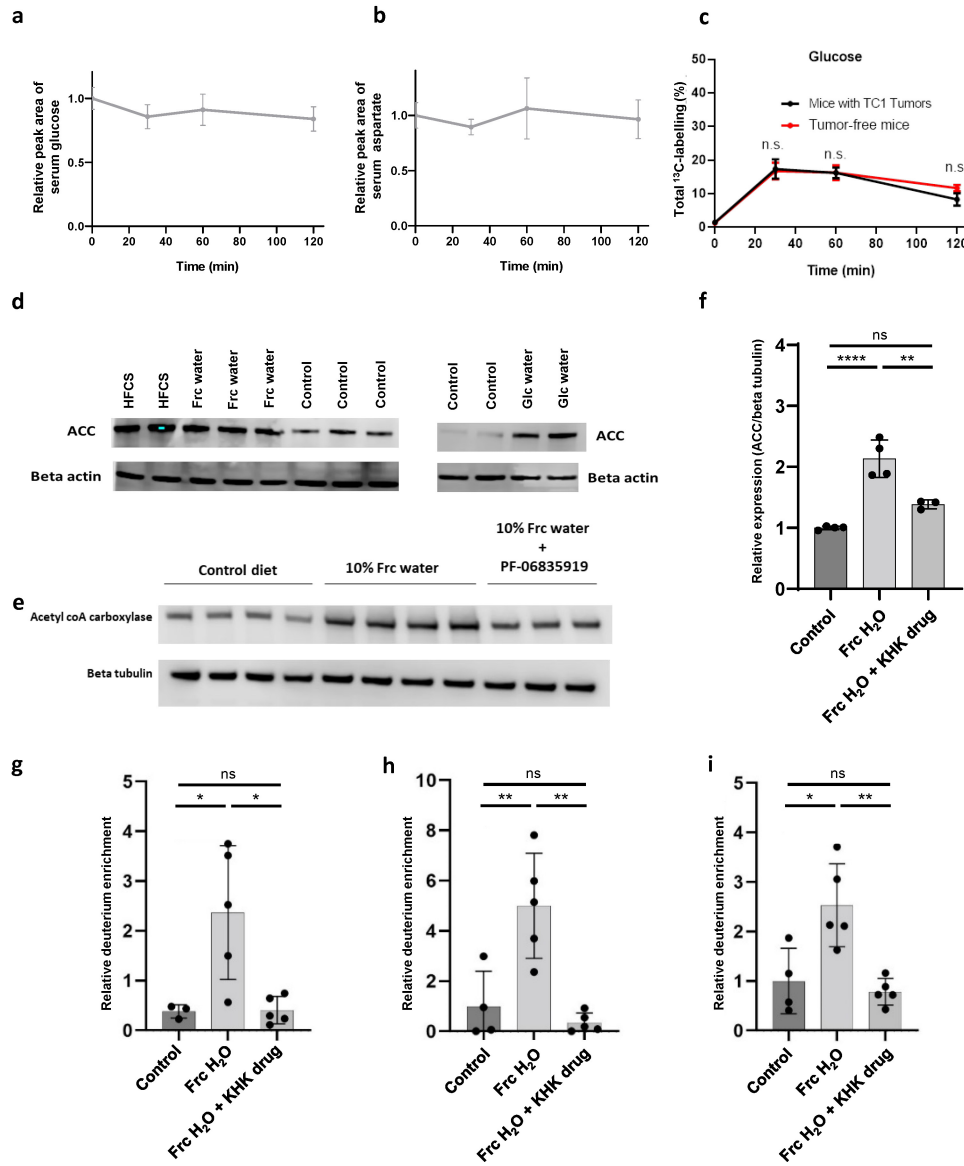
Extended Data Fig. 8 | Fructose is transformed into polar metabolites in a KHK-dependent manner. (a) Schematic for the generation of hepatocyte conditioned media (CM) and CaSki conditioned media (CM). Image created with BioRender.com. (b) Heatmap of labelled metabolites measured from hepatocyte CM (n = 3). White indicates no isotope labelling. Dark green indicates extensive isotope labelling. Except for fructose, which was the tracer, these metabolites were excreted into the media by primary mouse hepatocytes incubated for 24 h with [¹³C] fructose. (c) Heatmap of log₂ fold changes based on the ratio of metabolite intensity from CaSki CM relative to metabolite intensity from hepatocyte CM (n = 3). See (a) for design schematic. Dark blue indicates a low ratio (i.e., metabolite is high in hepatocyte CM and low in CaSki CM). Red indicates a high ratio (i.e., metabolite is low in hepatocyte CM and high in CaSki CM). Only metabolites from (b) that were at least 1% labelled were analysed. (d) Concentration of labelled fructose in the serum of nude mice 30 min after administration of 1.5 g/kg [¹³C] fructose and 75 min after the indicated dose of PF-06835919 (n = 3–4, per dose). (e) Isotopologue distribution for serum glucose from nude mice 30 min after administration of

[U-¹³C] fructose and 75 min after the indicated dose of PF-06835919 (n = 3–4, per dose). (f) Concentration of PF-06835919 in nude mouse serum after i.p. injection at a dose of 50 mg/kg. Measurements were made at 1 h, 4 h, 8 h, and 25 h post-injection (n = 4 mice per data point). Nonsignificant differences are not indicated. (g) CaSki tumour outgrowth in mice on a control diet administered a daily i.p. injection of vehicle (n = 4; Control Diet + No drug), a control diet administered 50 mg/kg PF-06835919 (n = 4; Control Diet + KHK Drug), or a high-fructose diet administered 50 mg/kg PF-06835919 (n = 3) Fructose Diet + KHK Drug). Data from Fig. 1g (Fructose Diet + No Drug, n = 7) provided a benchmark to show the impact of PF-06835919 on fructose-mediated CaSki tumour growth. All experiments from this figure were performed once. P values determined by ordinary one-way ANOVA with Tukey's multiple comparisons test (d, e) or ordinary one-way ANOVA with Tukey's multiple comparisons test of AUC (g). *P < 0.05, **P < 0.01, ***P < 0.001, ****P < 0.0001, and n.s. is not significant. (g) shows mean ± standard error. The rest of data shown as mean ± standard deviation.



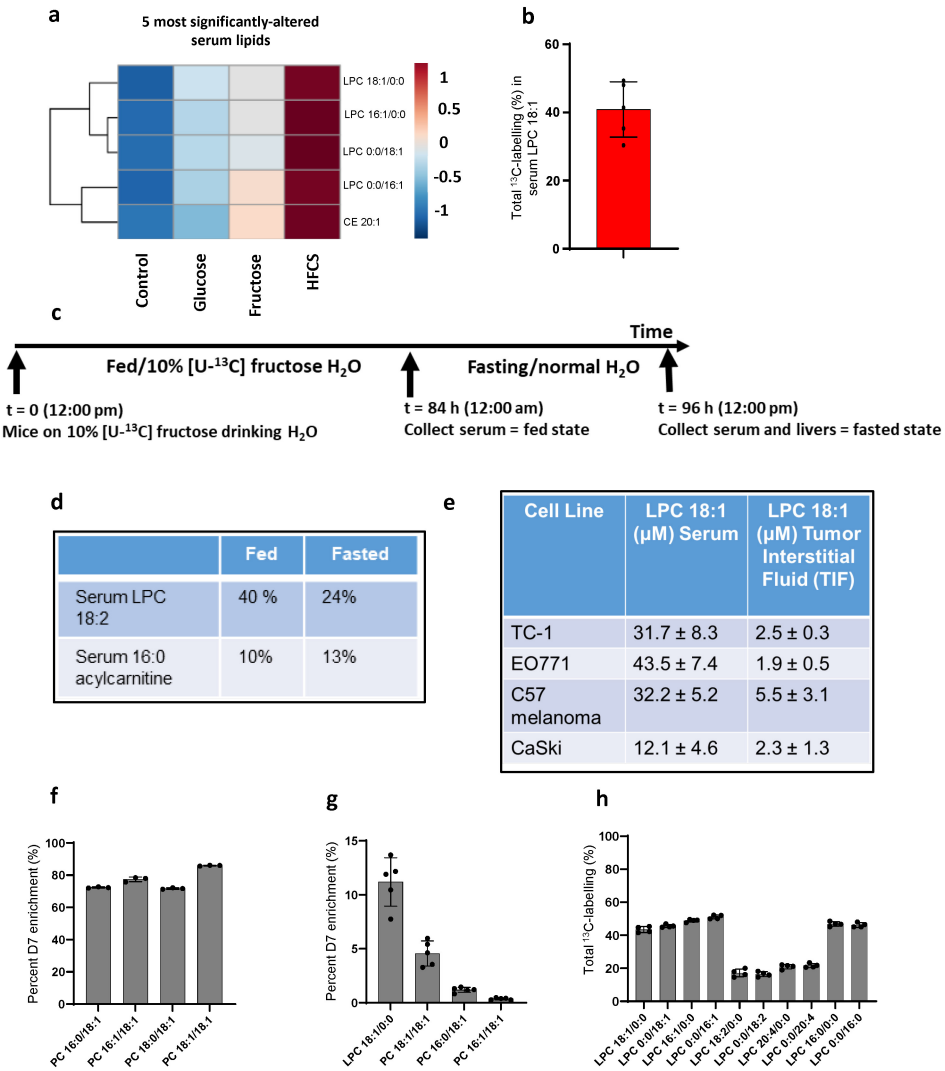
Extended Data Fig. 9 | Zebrafish express KHK-Cin a tissue distribution similar to mammals. (a) Comparison between human and zebrafish KHK transcripts. Zebrafish *khh-202* is analogous to *KHK-A* in humans, while zebrafish *khh-201* is analogous to *KHK-C* in humans. Inset shows an IGV view of KHK isoform expression in zebrafish brain, intestine, and testis. (b) Expression of KHK isoforms in zebrafish tissues. (c) Western blot analysis of aldolase B (aldob) from zebrafish livers. Succinate dehydrogenase (SDH) serves as a loading control. (d) Relative pool size of ¹³C-labelled fructose in serum after transferring fish to 20 mM [U-¹³C] fructose water following i.p. injection of vehicle (vehicle, n = 5) or after transferring fish to 20 mM [U-¹³C] fructose and 190 μM PF-06835919 water following an i.p. injection of 50 mg/kg PF-06835919 (PF-06835919, n = 5). One hour after i.p. injection of vehicle or PF-06835919, fish were placed in their respective fructose-labelled water condition for 12 h. (e) Tumour regrowth 10 days after tumour amputation from *BRAF/p53* zebrafish. Animals were housed in water containing fructose and vehicle (n = 5) or water containing fructose and 200 μM PF-06835919 (n = 4). (g) Relative pool of [U-¹³C] fructose from untreated (n = 6) or antibiotic-treated (n = 6–7) zebrafish intestine or serum 90 min after gavage with 1.5 g/kg [U-¹³C] inulin. Experiments from this figure were performed once. Pvalues determined by a two-sided T-test (d,e) or a Mann-Whitney Test (f). *P < 0.05, **P < 0.01, ***P < 0.001, ****P < 0.0001, and n.s. is not significant. Data in (g) shown as mean ± standard deviation. All other data shown as mean ± standard error.

vehicle (vehicle, n = 6) or after transferring fish to 20 mM [U-¹³C] fructose and 190 μM PF-06835919 water following an i.p. injection of 50 mg/kg PF-06835919, (PF-06835919, n = 5). One hour after i.p. injection of vehicle or PF-06835919, fish were placed in their respective fructose-labelled water condition for 12 h. (f) Tumour regrowth 10 days after tumour amputation from *BRAF/p53* zebrafish. Animals were housed in water containing fructose and vehicle (n = 5) or water containing fructose and 200 μM PF-06835919 (n = 4). (g) Relative pool of [U-¹³C] fructose from untreated (n = 6) or antibiotic-treated (n = 6–7) zebrafish intestine or serum 90 min after gavage with 1.5 g/kg [U-¹³C] inulin. Experiments from this figure were performed once. Pvalues determined by a two-sided T-test (d,e) or a Mann-Whitney Test (f). *P < 0.05, **P < 0.01, ***P < 0.001, ****P < 0.0001, and n.s. is not significant. Data in (g) shown as mean ± standard deviation. All other data shown as mean ± standard error.



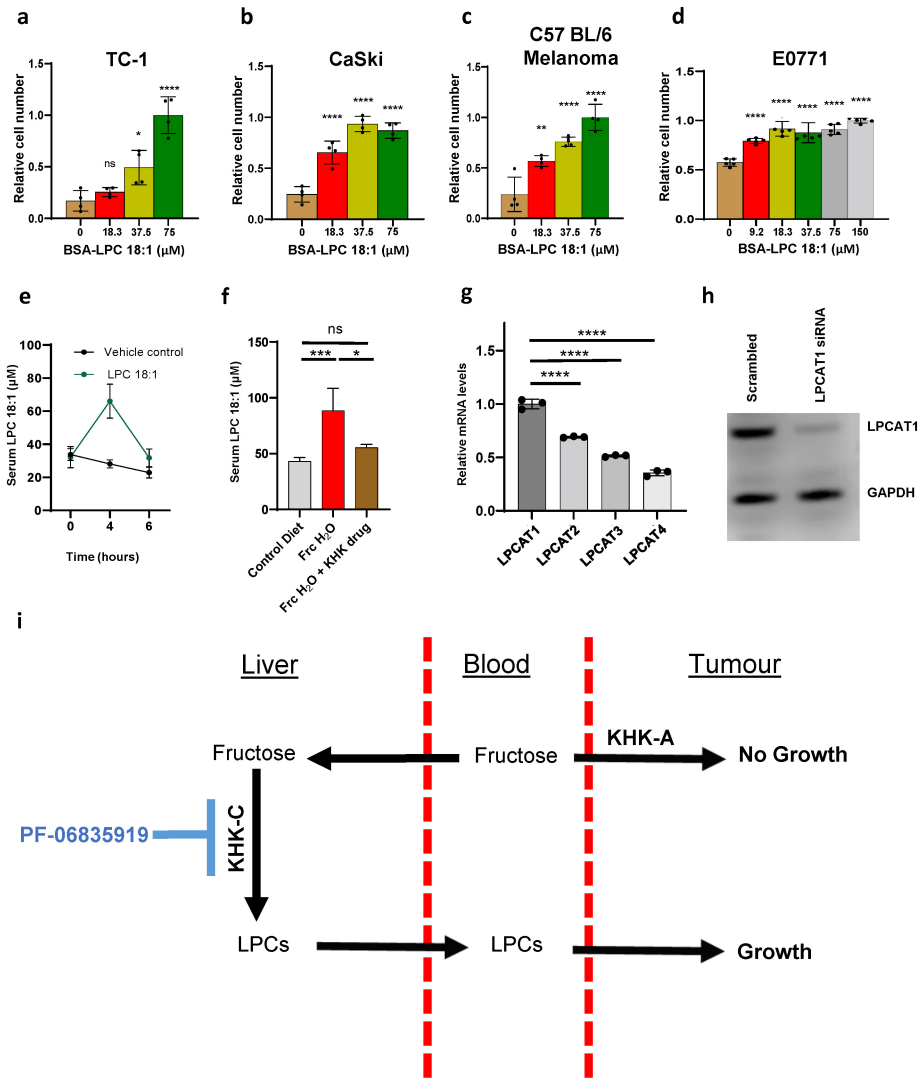
Extended Data Fig. 10 | Fructose enhances de novo lipogenesis but not circulating glucose and aspartate. (a) Relative total pool (sum of all labeled and unlabeled isotopologues) of serum glucose after gavaging C57BL/6 mice with 0.5 g/kg of [U^{13}C] fructose ($n = 4$) at $t = 0$. (b) Relative total pool (sum of all labeled and unlabeled isotopologues) of serum aspartate after gavaging C57BL/6 mice with 0.5 g/kg of [U^{13}C] fructose ($n = 4$) at $t = 0$. (c) Total ^{13}C -labelling in serum glucose after introducing 0.5 g/kg [U^{13}C] fructose via oral gavage to C57 BL/6 mice bearing TC-1 tumours ($n = 4$ in each condition). (d) Western blot analysis against acetyl-CoA carboxylase (ACC) from C57 BL/6 mouse livers after 6 weeks of a control diet supplemented with normal water (Control), 10% glucose water (Glc water), 10% fructose water (Frc water), or 20% HFCS (HFCS). (e) Western blot analysis of ACC from C57 BL/6 mouse livers after 5 days of a control diet supplemented with normal water (Control), 10% fructose water (10% Frc water),

or 10% fructose water + 50 mg/kg/day i.p. injection of PF-06835919 (10% Frc Water + PF-06835919). (f) Quantification of gel in (e), normalizing ACC band to the beta tubulin loading control. Relative deuterium enrichment for (g) hepatic palmitate, (h) hepatic stearate, and (i) hepatic oleate from C57 BL/6 mice given 50% D_2O for 12 h. Before the administration of D_2O , mice were pretreated with normal drinking water ($n = 3-4$), 10% fructose water ($n = 5$), or 10% fructose water + 50 mg/kg/day i.p. injection PF-06835919 ($n = 5$) for 7 days. The mice were maintained under these same conditions while administering 50% D_2O water. All experiments for this figure were performed once. P value determined by two-way ANOVA with Šídák's multiple comparisons test (c) or ordinary one-way ANOVA with Tukey's multiple comparisons test (e, g-i). * $P < 0.05$, ** $P < 0.01$, *** $P < 0.001$, **** $P < 0.0001$, and n.s. is not significant. All data shown as mean \pm standard deviation.



Extended Data Fig. 11 | Dietary fructose increases the availability of circulating lipids for the tumour. (a) Top 5 significant serum lipids from ANOVA. Data were collected from C57 BL/6 mice on control diets supplemented with normal water ($n = 4$), 10% glucose water (Glc water, $n = 4$), 10% fructose water (Fructose water, $n = 5$), or 20% HFCS (HFCS water, $n = 6$) for six weeks. Red indicates an increase in relative serum concentration. Blue indicates a decrease in relative serum concentration. (b) Total labelling for serum LPC 18:1 after providing C57 BL/6 mice ($n = 5$) access to 5% [U^{13}C] fructose water for 60 h. Data were corrected for natural ^{13}C abundance. (c) Schematic of labelling experiment for fed and fasted mice. Mice were given access to 10% [U^{13}C] fructose water for 84 h. (d) Fractional carbon atom labelling for serum 16:0 acylcarnitine and serum LPC 18:2 after administration of 10% [U^{13}C] fructose in the drinking water. Fed state was $t = 84$ h and fasting state was $t = 96$ h according to schematic in (c). Acylcarnitines provided an estimate of fatty acid labelling and LPC 18:2

an estimate of glycerol labelling. (e) Quantitative comparison of LPC 18:1 levels in the serum to matched tumour interstitial fluid (TIF) from multiple tumour types (TC-1, $n = 4$; EO771, $n = 5$; C57 BL/6 melanoma, $n = 3$; CaSki, $n = 3$). Data were collected from mice on a control diet for 4 weeks. (f) Percent of the indicated 18:1-containing PCs that incorporated 7 deuterium labels from the LPC 18:1-D7 tracer. Experiment was conducted by culturing CaSki cells ($n = 3$) with 20 μM LPC 18:1-D7 for 3 days. (g) Percent of the indicated 18:1-containing PCs in TC-1 tumours ($n = 5$) that incorporated 7 deuterium labels from the LPC 18:1-D7 tracer. See methods for detailed description of tracer administration. (h) ^{13}C -labelling for a variety of LPC species within the tumour. Data are from C57 BL/6 mice ($n = 4$) harbouring E6/E7-expressing TC-1 subcutaneous tumours. Mice were given access to 5% [U^{13}C] fructose water for 120 h. Data were corrected for natural ^{13}C abundance. All experiments from this figure were performed once. All data shown as mean \pm standard deviation.



Extended Data Fig. 12 | LPC18:1 enhances the proliferation of cancer cells.

(a-d) Relative cell number of indicated cell lines ($n = 4-5$ per dose) after treatment with different doses of BSA-LPC 18:1 for 4 days. (e) Quantitation of LPC 18:1 in the serum of C57 BL/6 mice after subcutaneous administration of one dose of 80 mg/kg LPC 18:1 ($n = 4$) or vehicle ($n = 4$). (f) Quantitation of LPC 18:1 in the serum of C57 BL/6 mice after 7-day administration of a control diet ($n = 5$), a control diet + 10% fructose water ($n = 5$), or a control diet + 10% fructose water + daily i.p. injection of 50 mg/kg PF-06835919 ($n = 3$). (g) Relative mRNA expression of *LPCAT* isoforms 1-4 in CaSki cells. (h) Western Blot analysis of LPCAT1 from CaSki cells 3 days after transfection with either LPCAT1 siRNA or scrambled control RNA. (i) Schematic overview of a mechanism by which fructose mediates tumour growth indirectly, by increasing the availability of fructose-derived nutrients to the tumour. We have shown that this mechanism

supports multiple animal models of skin, breast, and cervical cancer. Our results demonstrate that fructose is transformed into other nutrients such as LPCs by non-malignant, fructolytic tissues. Fructose-derived LPCs are transferred to the tumours, where they are used to support membrane synthesis. Beyond LPCs, it is likely that other fructose-derived nutrients are also transferred from fructolytic tissues to tumours. Inhibiting fructose metabolism in fructolytic tissues with PF-06835919 reduces circulating LPCs and slows the growth of tumours in animals consuming high levels of fructose. All experiments in this figure were performed once. P values determined by ordinary one-way ANOVA using Dunnett's test comparing all conditions to the control (a-d, g) and ordinary one-way ANOVA with Tukey's multiple comparisons test (f). $P < 0.05$, $^{**}P < 0.01$, $^{***}P < 0.001$, $^{****}P < 0.0001$, and ns. is not significant. All data shown as mean \pm standard deviation.

Corresponding author(s): Gary J. Patti

Last updated by author(s): Aug 14, 2024

Reporting Summary

Nature Portfolio wishes to improve the reproducibility of the work that we publish. This form provides structure for consistency and transparency in reporting. For further information on Nature Portfolio policies, see our [Editorial Policies](#) and the [Editorial Policy Checklist](#).

Statistics

For all statistical analyses, confirm that the following items are present in the figure legend, table legend, main text, or Methods section.

n/a Confirmed

- The exact sample size (n) for each experimental group/condition, given as a discrete number and unit of measurement
- A statement on whether measurements were taken from distinct samples or whether the same sample was measured repeatedly
- The statistical test(s) used AND whether they are one- or two-sided
Only common tests should be described solely by name; describe more complex techniques in the Methods section.
- A description of all covariates tested
- A description of any assumptions or corrections, such as tests of normality and adjustment for multiple comparisons
- A full description of the statistical parameters including central tendency (e.g. means) or other basic estimates (e.g. regression coefficient) AND variation (e.g. standard deviation) or associated estimates of uncertainty (e.g. confidence intervals)
- For null hypothesis testing, the test statistic (e.g. F , t , r) with confidence intervals, effect sizes, degrees of freedom and P value noted
Give P values as exact values whenever suitable.
- For Bayesian analysis, information on the choice of priors and Markov chain Monte Carlo settings
- For hierarchical and complex designs, identification of the appropriate level for tests and full reporting of outcomes
- Estimates of effect sizes (e.g. Cohen's d , Pearson's r), indicating how they were calculated

Our web collection on [statistics for biologists](#) contains articles on many of the points above.

Software and code

Policy information about [availability of computer code](#)

Data collection Not applicable

Data analysis Statistical analyses were performed by using GraphPad Prism 9.2 for Windows. For untargeted metabolomics, data processing was accomplished by using XCMS. Centroided peaks were uploaded to MetaboAnalyst 5.0. Lipid species were annotated by uploading MS/MS spectra into Agilent MassHunter Lipid Annotator 1.0. Raw metabolomics data were analyzed with Qualitative Navigator B.08.00 and Skyline (version 20.1.0.155). RNA-seq reads were aligned to the Genome Reference Consortium Human Build 38 (GRCh38) using STAR2 with Ensembl genes for homo sapiens version 90. Isoform expression levels for KHK-A and KHK-C were calculated and normalized as Fragments Per Kilobase per Million reads (FPKM) by using Cufflinks with default parameters. Integrative genomics viewer (IGV) was used to visualize and manually inspect sequencing reads from isoform specific exons.

For manuscripts utilizing custom algorithms or software that are central to the research but not yet described in published literature, software must be made available to editors and reviewers. We strongly encourage code deposition in a community repository (e.g. GitHub). See the Nature Portfolio [guidelines for submitting code & software](#) for further information.

Data

Policy information about [availability of data](#)

All manuscripts must include a [data availability statement](#). This statement should provide the following information, where applicable:

- Accession codes, unique identifiers, or web links for publicly available datasets
- A description of any restrictions on data availability
- For clinical datasets or third party data, please ensure that the statement adheres to our [policy](#)

Provide your data availability statement here.

Research involving human participants, their data, or biological material

Policy information about studies with [human participants or human data](#). See also policy information about [sex, gender \(identity/presentation\), and sexual orientation](#) and [race, ethnicity and racism](#).

Reporting on sex and gender	Given that a focus of our work is cervical cancer, which exclusively occurs in women, we only considered female sex.
Reporting on race, ethnicity, or other socially relevant groupings	We did not report on race, ethnicity, or other socially relevant groupings in our study.
Population characteristics	All patients had cervical cancer in this cohort and were uniformly treated with curative-intent chemoradiation and clinical data were prospectively collected
Recruitment	Cervical cancer patients were enrolled in a prospective tumor banking study with written informed consent. Self-selection bias is not likely to impact our RNA-seq and overall survival data
Ethics oversight	Washington University Institutional Review Board (IRB). IRB number is 201105374

Note that full information on the approval of the study protocol must also be provided in the manuscript.

Field-specific reporting

Please select the one below that is the best fit for your research. If you are not sure, read the appropriate sections before making your selection.

Life sciences Behavioural & social sciences Ecological, evolutionary & environmental sciences

For a reference copy of the document with all sections, see nature.com/documents/nr-reporting-summary-flat.pdf

Life sciences study design

All studies must disclose on these points even when the disclosure is negative.

Sample size	Sample sizes were based on previous experimental experience in our research group and on previous studies in the literature
Data exclusions	A Grubb's Test was used to determine if outliers were present in the data. It was determined that one data point from the control condition of Figure 1A was an outlier, which was multiple-fold higher than the average of that condition. This single data point was removed.
Replication	Each experimental finding reported was determined by using multiple animals or cell-culture experiments. The data were reproducible.
Randomization	Mice bearing tumors were randomly assigned to different dietary conditions. Zebrafish with resected tumors were randomly assigned to the high-fructose or control conditions. When assessing tumor xenograft outgrowth in mice under two different experimental conditions, initial tumor sizes were assessed to confirm that there were no statistically significant differences in initial tumor sizes between groups.
Blinding	Samples were prepared for metabolomics, analyzed by LC/MS, and the resulting data processed in a blinded fashion

Reporting for specific materials, systems and methods

We require information from authors about some types of materials, experimental systems and methods used in many studies. Here, indicate whether each material, system or method listed is relevant to your study. If you are not sure if a list item applies to your research, read the appropriate section before selecting a response.

Materials & experimental systems

n/a	Involved in the study
<input type="checkbox"/>	<input checked="" type="checkbox"/> Antibodies
<input type="checkbox"/>	<input checked="" type="checkbox"/> Eukaryotic cell lines
<input checked="" type="checkbox"/>	<input type="checkbox"/> Palaeontology and archaeology
<input type="checkbox"/>	<input checked="" type="checkbox"/> Animals and other organisms
<input type="checkbox"/>	<input checked="" type="checkbox"/> Clinical data
<input type="checkbox"/>	<input checked="" type="checkbox"/> Dual use research of concern
<input checked="" type="checkbox"/>	<input type="checkbox"/> Plants

Methods

n/a	Involved in the study
<input checked="" type="checkbox"/>	<input type="checkbox"/> ChIP-seq
<input checked="" type="checkbox"/>	<input type="checkbox"/> Flow cytometry
<input checked="" type="checkbox"/>	<input type="checkbox"/> MRI-based neuroimaging

Antibodies

Antibodies used

anti-ketohexokinase (Santa Cruz; catalog number: sc-377411), anti-ketohexokinase-C (Signalway; catalog number 21709), anti-ketohexokinase-A (Signalway; catalog number: 21708), anti-sorbitol dehydrogenase (Santa Cruz; catalog number: sc-377200), antialdolase B (Santa Cruz; catalog number: 393278); anti-beta tubulin (Cell Signaling; catalog number: 2128), anti-lysophosphatidylcholine acyltransferase 1 (Proteintech; catalog number: 16112-1-AP); anti-glyceraldehyde 3-phosphate dehydrogenase (Cell Signaling; catalog number: 3683S); or anti-succinate dehydrogenase (Cell Signaling; catalog number: 5839S)

Validation

All antibodies used in the study had validating data on the antibody on the supplier website. Furthermore, the antibodies have been used in other publications

Eukaryotic cell lines

Policy information about [cell lines and Sex and Gender in Research](#)

Cell line source(s)

HeLa cells were obtained from the Tissue Culture Support Center of Washington University in St Louis. CaSki and Siha cells were obtained from the laboratory of Julie Schwarz. E6, E7-expressing TC-1 cells were obtained from the laboratory of TC Wu. BrafV600E-mutant, Pten-deficient mouse melanoma cells were obtained from the laboratory of George Souroullas and were derived from TyCreERT2 Braf V600E/+ PtenF/F genetically engineered C57 BL/6 mouse models. A-498 cells were obtained from the laboratory of James Hsieh. MIA PaCa-2 cells were obtained from the laboratory of William Hawkins. Huh7 cells were obtained from the laboratory of Brian Finck. Z crest C zebrafish melanoma cells were obtained from the laboratory of Charles Kaufman. E0771 (94A001) were obtained from CH3 BioSystems. MCF-7 (HTB-22) and 3T3-L1 (CL-173) cells were obtained from American Type Culture Collection

Authentication

Cell lines from American Tissue Type Collection (ATCC) were authenticated by ATCC

Mycoplasma contamination

Cell lines tested negative for Mycoplasma

Commonly misidentified lines (See [ICLAC](#) register)

HeLa

Animals and other research organisms

Policy information about [studies involving animals; ARRIVE guidelines](#) recommended for reporting animal research, and [Sex and Gender in Research](#)

Laboratory animals

Nude mice; Athymic strain (CRL strain code: 490); female, studies were begun when mice were 12-14 weeks old. C57 BL/6J (strain number: 000664) female mice. Studies were begun when mice were 10-14 weeks old.

Wild animals

Not applicable

Reporting on sex

For the use of our cervical cancer and breast cancer models, female mice were the most relevant sex to use. Furthermore, female mice bearing tumors were used in this study as they were protected from insulin resistance and obesity when consuming high amounts of sugar. This allowed us to decouple the effects of insulin resistance and obesity from our observations of sugar-mediated tumor growth enhancement.

Field-collected samples

Not applicable

Ethics oversight

All procedures were approved by the Washington University Institutional Animal Care and Use Committee

Note that full information on the approval of the study protocol must also be provided in the manuscript.

Clinical data

Policy information about [clinical studies](#)

All manuscripts should comply with the ICMJE [guidelines for publication of clinical research](#) and a completed [CONSORT checklist](#) must be included with all submissions.

Clinical trial registration Not applicable; study was not a clinical trial but rather a tumor prognostic study and a validation study of isoforms of KHK and aldolase B in human cervical tumors

Study protocol The Institutional Review Board (IRB) protocol number is 201105374

Data collection Data were collected at Washington University School of Medicine

Outcomes Primary outcomes measured were KHK-A, KHK-C, and aldolase (A, B, and C isoforms) expression. Overall survival and KHK-A expression relative to tumor stage were also measured

Plants

Seed stocks

Report on the source of all seed stocks or other plant material used. If applicable, state the seed stock centre and catalogue number. If plant specimens were collected from the field, describe the collection location, date and sampling procedures.

Novel plant genotypes

Describe the methods by which all novel plant genotypes were produced. This includes those generated by transgenic approaches, gene editing, chemical/radiation-based mutagenesis and hybridization. For transgenic lines, describe the transformation method, the number of independent lines analyzed and the generation upon which experiments were performed. For gene-edited lines, describe the editor used, the endogenous sequence targeted for editing, the targeting guide RNA sequence (if applicable) and how the editor was applied.

Authentication

Describe any authentication procedures for each seed stock used or novel genotype generated. Describe any experiments used to assess the effect of a mutation and, where applicable, how potential secondary effects (e.g. second site T-DNA insertions, mosaicism, off-target gene editing) were examined.